Spring 2016

Oxidation Resistance of Nanocrystalline 316L Stainless Steel Processed by High Pressure Torsion

Kevin J. Meisner
kjm69@zips.uakron.edu

Oxidation Resistance of Nanocrystalline 316L Stainless Steel Processed by High Pressure Torsion

4250:947 Honors Project

Author: Kevin Meisner

Advisor: Dr. Rajeev Gupta
Readers: Dr. Scott Lillard, Dr. Gregory Morscher

Fall 2015 and Spring 2016

Table of Contents

1. Executive Summary

1.1 Problem Statement

A literature review and experimental studies were performed to assess the possibility of improving the high temperature oxidation resistance of stainless steel 316L using a processing technique called high pressure torsion (HPT). A thorough literature review made me hypothesize that HPT can be used to refine grains to nanocrystalline size and will likely decrease oxidation rates of stainless steel in air. If true, this processing method may help increase the lifetime of engineered parts made of stainless steel (316L in this study) being used in high temperature environments. It is expected that an increased asset lifetime will save on costs over the long term.

In order to investigate the high temperature oxidation behavior, the oxidation tests were conducted in a furnace. While oxidation in other environments such as SO_2, steam, etc. may give more complete data on high temperature performance, all experiments performed were in air due to equipment and safety limitations. Changes in the weight of the metal sample at regular time periods were measured to investigate the oxidation kinetics. Afterwards, cross sections and surfaces of the samples were characterized using scanning electron microscope to provide additional details on the oxidation mechanisms.

1.2 Summary of Results and Conclusions

The oxidation tests were performed at 600, 800, and 900°C in a box furnace. Furnace testing did not necessarily confirm the hypothesis that nanocrystalline 316L produced by HPT exhibits decreased oxidation rates compared to its microcrystalline counterpart, at least at the

temperatures tested (800 and 900°C). Table 1, in the "Discussion" section, succinctly reports the oxidation rate constants for each material at each temperature. As can be seen, the oxidation rate constants for the nanocrystalline, processed material were nearly equal or possibly greater than those for the unprocessed, microcrystalline material. These rate constants were the slope of the trend line in a plot of the square of weight change versus time (see Figure 30). The R^2 values indicate that all tests exhibited a parabolic rate law, which is expected for these materials (as described in later sections). More recent oxidation experiments conducted for significantly longer period of time indicated decrease in spallation tendency due to HPT. However, detailed studies are required to reach to any conclusion.

Scanning electron microscope (SEM) coupled with energy dispersive X-ray spectroscopy (EDXS) was used to characterize the oxide scale. No major significant difference between the two materials in oxide thickness or other cross-sectional features was observed. However, it is possible that the scale of the microcrystalline (mc) substrate had a greater tendency of crack and spall than that of the nanocrystalline (nc) substrate. When samples were removed from the furnace, more spalling debris were found near the mc sample than the nc sample, as shown in Figure 24. Optical microscope images show spallation regions in both samples where grey metal is exposed. Figure 25 shows that these spallation regions cover a greater portion of the surface on the mc sample compared to the nc sample.

It is difficult to draw any definite conclusions from the data. The hypothesis that HPT will increase oxidation resistance was not confirmed. It appears that HPT resulted in a more adherent

scale after oxidation, but this difference does not directly translate into improved oxidation performance and further studies are required.

1.3 Implications

The results, which show no significant decrease in oxidation rates for HPT processed 316L, are interesting when compared to literature which shows beneficial effects of nanocrystallinity in other chromia-forming materials[1]. There are several possible explanations for this discrepancy, including the possibility of grain growth at the temperatures tested, thereby losing its nanocrystalline structure[2–5]. Another possibility is that HPT introduces some unknown metallurgical features, not present in the material produced by other grain refinement processing methods, that is detrimental to oxidation resistance. It will take more studies to explain the results of HPT found in this report.

This project taught the skills of materials characterization using SEM, EDXS, and possibly in the future, XPS. It familiarized me with the literature on high temperature oxidation, nanocrystalline materials, and gave me greater familiarity with reading and understanding scientific papers. It taught all the skills relevant with materials testing such as sample preparation, designing an experimental procedure, and making accurate measurements. Importantly, it also taught me how to carefully draw conclusions from my data without making spurious conclusions not supported by the results.

2.0 Introduction

Material degradation due to the high temperature oxidation is a great concern in a variety of applications including nuclear power, solid oxide fuel cells, fossil fuel plants, thermoelectric devices, and concentrating solar power[6]. At service temperatures, thermodynamic driving forces may be significant and kinetics of chemical processes may be relatively fast, posing challenges to design and manufacture materials for such environments[1]. Suitable materials typically develop protective oxide scales that serve as barriers between the substrate and the oxidizing environment[7]. Once a protective scale is formed, kinetics of oxidation are then controlled by diffusion of oxygen, metal cations, and point defects through the scale[7]. Diffusivities may be dependent on chemical and physical properties of both the substrate and scale. One such property is grain size[1,8–11]. Formation of an external oxide scale is dependent on diffusion of more reactive solutes (Cr in the case of 316L) from the bulk of the material to the surface[7,8]. In short, refining the grain size to an average of tens of nanometers in diameter may facilitate diffusion of these solutes due to the higher volume fraction of grain boundaries and triple points, where diffusivities are much greater[1,8].

The unique properties of nanocrystalline materials are associated with a very fine grain size and a large number of structural defects, i.e., grain boundaries and triple points. Such a high fraction of structural defects in nanocrystalline materials can lead to a significant increase in stored energy, which may increase reactivity. This phenomenon is expected to have a dual effect on oxidation behavior as described in [8]. Moreover, the processing route and processing parameters used to produce nanocrystalline materials is expected to have strong influence on the structure and therefore on the properties. For instance, the electrochemical corrosion behavior of

the nanocrystalline stainless steel is reported to be strongly influenced by the processing route[12]. Therefore, the oxidation behavior of various materials produced by various processing routes should be studied in various environments to understand the influence of nanocrystalline structure and processing route.

There are a number of processing methods to refine the grain size, but the method examined here is called High Pressure Torsion, or HPT. The HPT process will be described in detail in later sections, but in short it involves the application of simultaneous axial and torsional strain to a metal sample[13–15]. The intent is to examine the influence grain refinement due HPT on the high temperature oxidation performance of stainless steel 316L.

3.0 Background and Literature Review

The literature review was a significant part of this project and so will be reported in depth here.

High pressure torsion (HPT) is a metals processing technique involving plastic deformation from simultaneous axial compression and torsional strain. While the technique dates back to several decades ago, HPT gained renewed interest in the past twenty to thirty years when its potential for grain refinement to nanoscale, leading to the production of ultrafine-grained (UFG) and nanocrystalline (NC) metals, with desirable mechanical properties was recognized[13]. UFG and NC materials, produced via HPT exhibited enhanced mechanical properties including increased fatigue strength and hardness[16]. The properties of materials processed by HPT can be further enhanced through post processing such as annealing[17]. Grain refinement to nanoscale is reported to impart a high volume fraction of atoms located at grain boundaries[8]. Atoms at grain boundaries possess high energy and grain boundaries offer a faster diffusion path leading to significant increase in diffusion. This has implications for phenomena dependent on diffusion of species, particularly oxidation[8].

3.1 High Pressure Torsion – A Description of the Technique

Figure 1 shows a schematic of a system used for HPT processing[15]. During processing, a disk-shaped sample of the material to be formed is placed between upper and lower anvils. Two concurrent strains are applied to the sample – one axial and one torsional. The severe plastic deformation (SPD) induced in the sample results in UFG or NC materials. Literature comparing various SPD processes suggests that HPT may be more effective at producing NC materials than

other processing methods, as grain resulting from HPT have been shown to be significantly smaller at approximately 90 nm[15]. The resulting microstructure has been reported to be a function of various parameters including applied pressure (P in Figure 1), number of rotations, radius of the test specimen, etc. To achieve grain refinement to ~100 nm, pressures of 5 GPa and 5 rotations are typical[15]. The HPT specimens used in the experimental section of this report were processed at 10 GPa and 10 rotations.

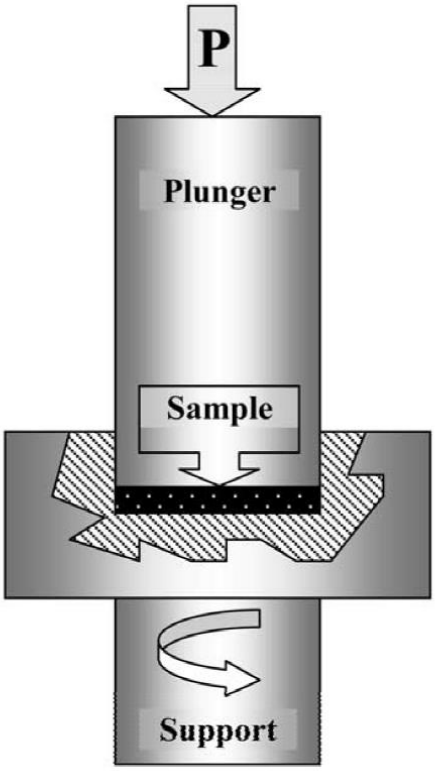

Figure 1 – Schematic of HPT Processing[15]

Transmission electron microscopy (TEM) has been widely used to study the physical mechanisms responsible for grain refinement caused by HPT[14]. The grain refinement process

appears to occur in distinct stages, the first being plastic deformation by glide and multiplication of dislocations[14]. After further deformation, twinning and shear-banding on the microscale develop parallel to the direction of torsion. Twin grains begin to intersect and form rhombic block structures with high dislocation densities at their edges[14]. This prevents further plastic deformation by dislocation glide and deformation proceeds instead by sub-micron sized shear banding[14]. The twins begin forming twin-matrix lamellar structures that are then further refined into the resulting nano-sized grains[14]. The final grain size is a function of the total strain accumulated through all the processes described above.

The true accumulated strain of the HPT sample may be approximated by Equation 1, which assumes a disk-shaped sample with a radius much greater than the height[13]. ε is the accumulated strain, N is the number of rotations about the axis, r is the radius of the disk sample, and h is the height of the sample[13]. As can be seen, the resulting strain is a function of the radius Therefore, the microstructure (particularly grain size) and thus material properties (e.g., hardness) are also a function of radius[14].

$$\varepsilon = \ln\left(\frac{2\pi N \cdot r}{h}\right) \qquad \text{Equation 1}$$

An example of property dependence on radius is presented in Figure 2[14]. The plot is of 316L HPT samples with number of turns N = 5 and N=45. (RT corresponds to processing at room temperature and N2 corresponds to processing at -196°C. Use of HPT at such low temperatures is outside the scope of this project). A clear relationship can be seen with decreased hardness (and less grain refinement) near the center. The effect becomes less pronounced with a greater

number of turns, suggesting the material may become nearly homogenous if processed with a sufficient number of turns[14]. A more homogeneous structure may also be accomplished with greater axial load (with 9 GPa being a typical value yielding nearly homogenous microstructure)[13].

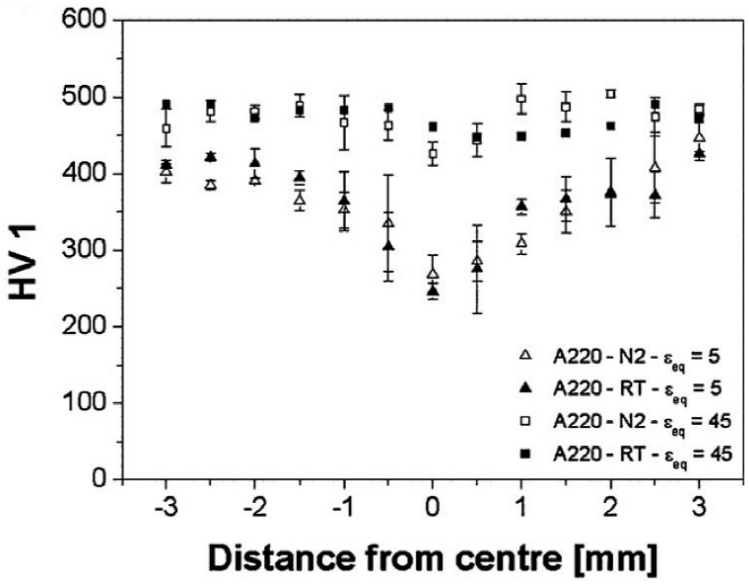

Figure 2 – Vicker's Hardness as a function of radius 316L, processed at two temperatures. [14]

Grain size difference between the center and periphery of an HPT sample can be seen in Figure 3[15]. At P = 1 GPA the grains near the sample's center (top) are noticeably coarser than the grains near the sample's periphery (bottom). At larger axial stresses, the difference between the grain size at center and periphery becomes less noticeable. At an applied stress of 9 GPa there is little difference in grain size from center to periphery[15].

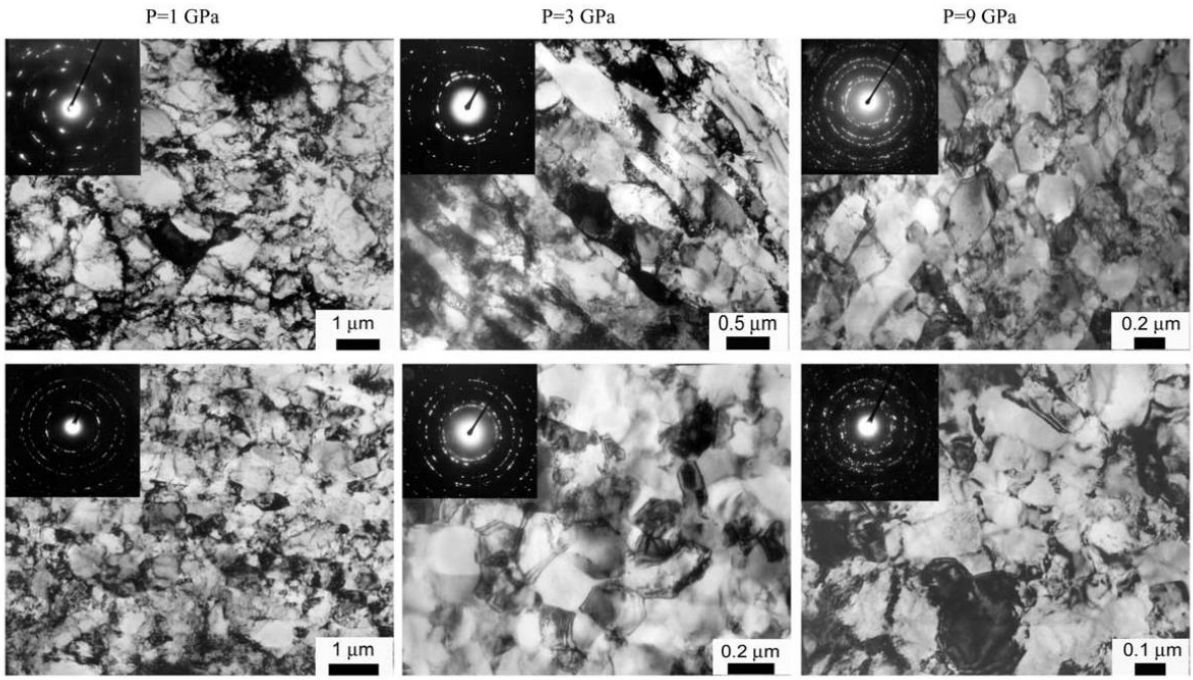

Figure 3 –Microstructure and SAED patterns as function of axial stress and distance from center (1st row: near center, 2nd row: near periphery)[15]

3.2 Effects of Grain Size on High Temperature Oxidation

The effects of grain size on high temperature oxidation of alloys are complex due to competing effects of diffusion of metal atoms and metal vacancies, oxygen diffusivity, the possible formation of secondary and ternary scales, mechanical properties of the scales, solubility of oxides, alloying additions etc[7]. Because of the variety of factors, grain refinement may increase, decrease, or not affect corrosion rates, depending on the material and environment. For example, studies of copper oxidation at 300-700 °C showed that nanocrystalline copper may oxidize faster than its course-grained counterparts[18], but nanocrystalline SS304 typically oxidizes slower than course-grained SS304 at 900 °C[19]. As can be seen, one must take into consideration a variety of factors when trying to predict effect of grain size on oxidation behavior.

An important effect of grain size is volume fraction of atoms at grain boundaries. In a polycrystalline material, atoms may be thought of occupying crystalline regions (within the bulk of grains) or intercrystalline regions (at grain boundaries, including triple points where three grains contact at a point)[8]. Polumbo, et. al. proposed Equation 2 relating atom fraction in intercrystalline regions (V_t^{ic}), grain diameter (specifically, the diameter of the largest inscribed sphere, d) and grain boundary thickness (δ)[20].

$$V_t^{ic} = 1 - \left[\frac{d-\delta}{d}\right]^3 \qquad \text{Equation 2}$$

From Equation 2 one can find relations for grain boundary volume fraction (V_t^{gb}) and triple point volume fraction (V_t^{tp})[8].

$$V_t^{gb} = \left[\frac{3\delta(d-\delta)^2}{d^3}\right] \qquad \text{Equation 3}$$

$$V_t^{tp} = V_t^{ic} - V_t^{gb} \qquad \text{Equation 4}$$

Figure 4 plots intercrystalline volume fraction versus grain size assuming a grain boundary thickness of 1 nm[20]. As grain size approaches 10 nm, volume fraction of intercrystalline regions can become significant, exceeding 0.1.

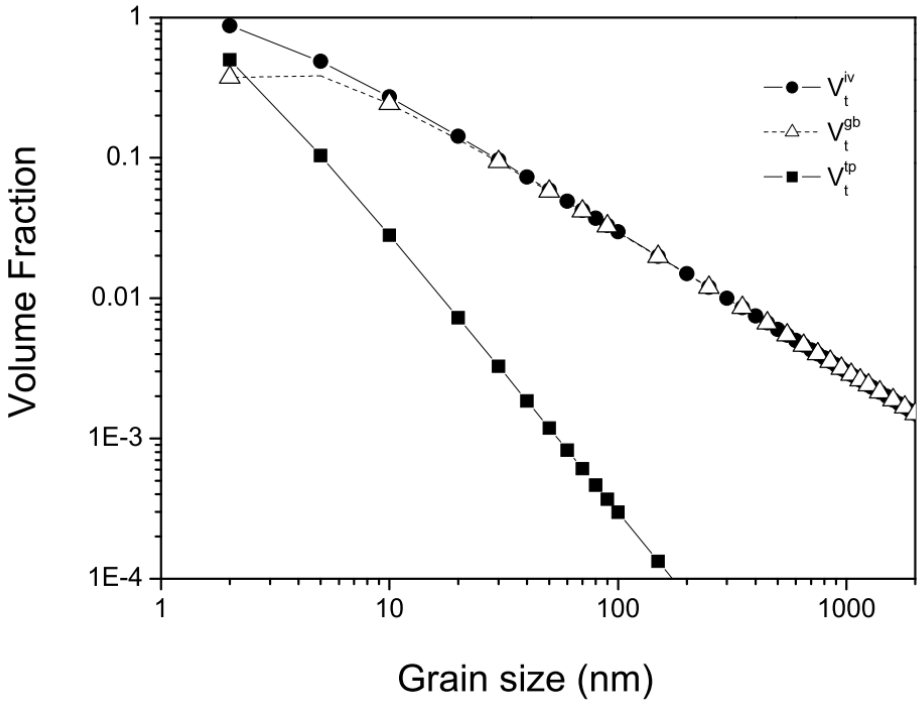

Figure 4 – Volume fraction of grain boundaries, triple points, and intercrystalline region vs. grain size assuming a grain boundary thickness of 1 nm[20]

Typically the activation energy for diffusion through the lattice of a bulk grain is significantly greater than the activation energy for "short-circuit" diffusion (diffusion through grain boundary/intercrystalline regions). One can find an effective diffusion constant using atom fraction in the boundaries *f*, lattice diffusion constant D_L, and grain boundary diffusion constant D_B[8,18]:

$$D_{eff} = (1-f)D_L + fD_B \qquad \text{Equation 5}$$

The effective diffusion constant of solutes has implications for the oxidation process. For materials forming external protective scales, increased flux of solute due to grain refinement may

increase oxidation resistance. External oxides of aluminum and chromium may be denser, and more adherent in nanocrystalline alloys and therefore limit oxidation kinetics through diffusion of species through the scale[8]. To form and maintain such a protective scale, a critical concentration of solute (typically Cr or Al) is required[1]. Internal oxidation occurs below a critical concentration of solute, which is typically not protective as it does not result in an external scale. The critical concentration of solute B (N_B) required to form and maintain an oxide scale is a function of the valence of B atoms (Z_B), the atomic weight of oxygen (M_o), the diffusion constant of B in the alloy (D_B), and the parabolic rate constant (k_p)[1]:

$$N_B = \frac{V}{Z_B M_o}\left(\frac{\pi k_p}{D_B}\right)^{\frac{1}{2}} \qquad \text{Equation 6}$$

From Equation 6 it is seen that as D_B increases, N_B decreases. Thus, a process that increases the effective diffusivity of B will lower the critical concentration of B in the bulk required to form a protective, external oxide scale. Singh Raman, et. al. have modeled the ratio of this critical amount of chromium (ratio is to amount of Cr required for 1.5μm grains at 350 °C) as a function of grain size[1]. The results are shown in Figure 5.

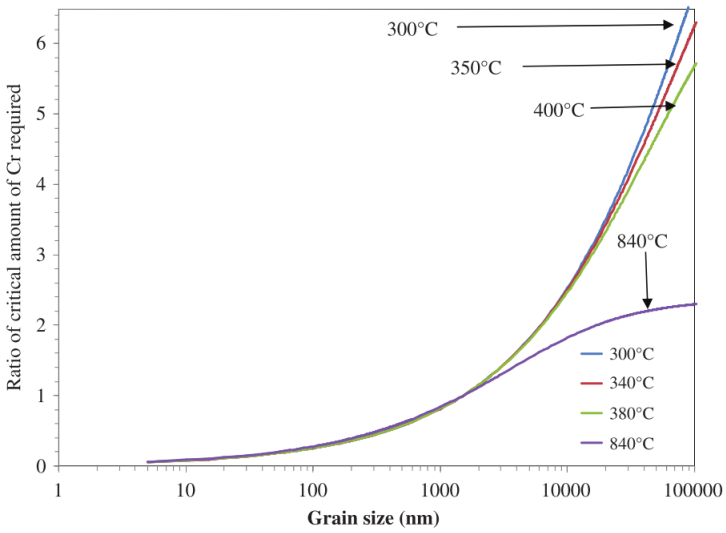

Figure 5 – Ratio of critical amount of Cr required for external oxidation of a Fe-Cr alloy (assumes grain size of 1.5μm and T=350 °C)

Experimental measurements of oxidation kinetics of Fe-Cr materials suggest smaller grain can indeed increase high temperature oxidation resistance. Figure 6 shows weight gain per unit area for oxidation of microcrystalline and nanocrystalline (produced by high-energy ball milling followed by consolidation) Fe-10Cr alloys at 400°C[1]. The oxidation rate of nanocrystalline materials was reported to be an order of magnitude less than that of the corresponding microcrystalline materials. Both materials displayed parabolic kinetics, suggesting that the rate limiting step in oxidation is transport through an external oxide scale. In the same study, secondary ion mass spectrometry (SIMS) suggested the presence of a more robust, protective external oxide scale on the nc samples[1].

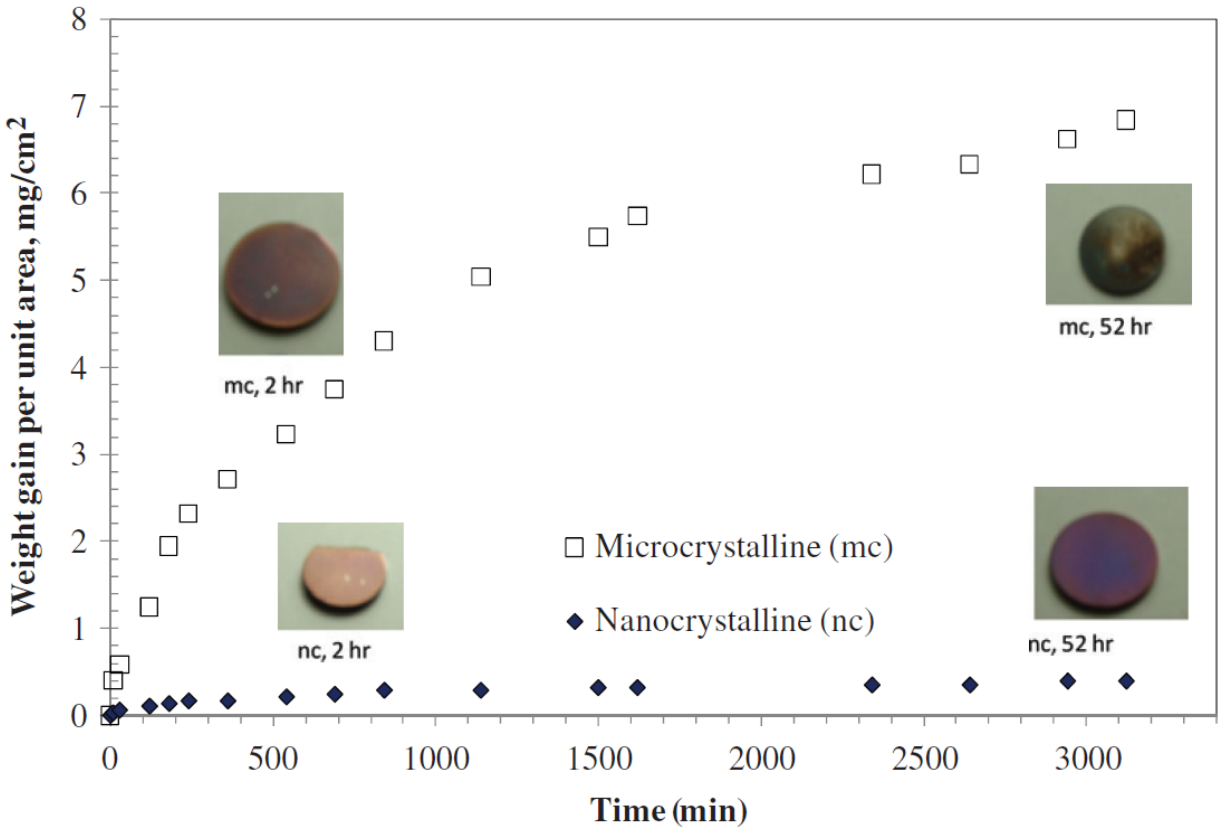

Figure 6 – Oxidation kinetics of nano- and micro-crystalline Fe-10Cr at 400 °C [1]

Grain refinement to nanoscale has been reported to increases oxidation resistance of chromia forming alloys (i.e. Fe-10Cr) because of enhanced diffusion contributes to the formation of a protective chromia scale. However, the effect of grain size is complex and decreased grain size is not beneficial for all materials. Early studies on the oxidation of nickel show that decreased grain size, created through cold working, can actually increase oxidation rates, as shown in Figure 7 below[10].

Nickel (II) oxide is a p-type, cation-deficient semiconductor[7] and so oxidation occurs through diffusion of cation vacancies and electron holes through the external NiO scale. SEM images of the surfaces and cross-sections of oxidized nickel show that cold-worked (i.e. finer grain)

samples form finer grained oxide scales[10]. The authors suggested that the finer grains allow for faster transport of diffusing species through the scale and therefore greater oxidation rates[10]. This leads to a difficult situation where finer grain size may lead to both greater diffusion of species in the bulk, which is beneficial, and/or greater diffusion of species through the scale, which is detrimental. This demonstrates that reduced grain size can have multiple simultaneous effects, some competing, that make it difficult to predict the net effect of grain size on oxidation rate.

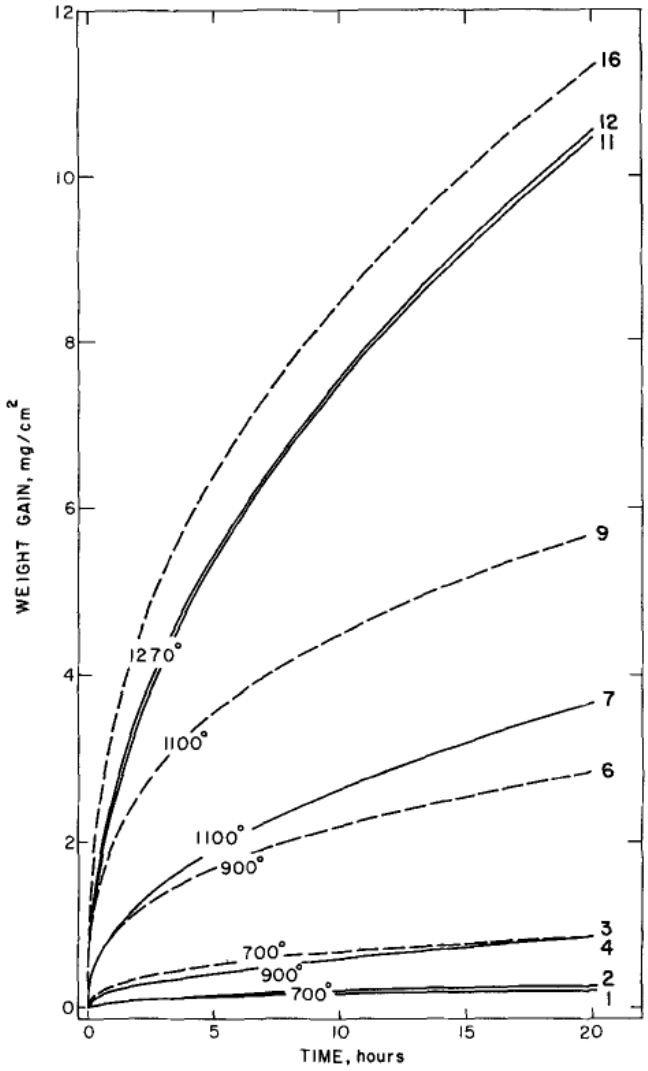

Figure 7 – Oxidation rates of cold-worked (dashed lines) and annealed (solid lines) nickel[10].

Though the effect of grain size is complex, the literature suggests that oxidation rates of nanocrystalline 316L formed by HPT will be less than oxidation rates of traditional, microcrystalline 316L. Nanocrystalline materials that depend on an external oxide, such as type 304 stainless steel[19], some magnesium rare earth alloys[21], ferritic Fe-Cr steels[1], and Fe-Cr-Ni alloys containing zirconium additions[22]. Because 316L develops a protective chromia scale and because studies with similar chromia-forming materials benefit from grain refinement, it is hypothesized that 316L will benefit from grain refinement by HPT. However, most of the results in the literature are for processing methods other than HPT such as high-energy ball milling[1,22] and severe rolling[19]. It is unknown if HPT may introduce some other variable that may affect oxidation behavior. More recent review on the corrosion behavior of nanocrystalline stainless steel indicated that the properties of nanocrystalline materials not only depend upon the nanocrystalline structure but also upon the processing route employed[12]. Therefore, there is merit in studying the effects of high press torsion on high temperature oxidation resistance of stainless steel.

3.3 Grain Growth at High Temperatures

Nanocrystalline materials are particularly vulnerable to grain growth at high temperatures because of the high concentration of non-equilibrium defects introduced during processing[23]. Therefore, grain size must be stabilized if the desirable properties of the nanocrystalline material are to be preserved. The driving force for grain growth is the relatively high energies of intercrystalline regions (i.e. grain boundaries) compared to crystalline regions within the bulk of the grains. Some attempts to reduce grain growth have focused on reducing growth kinetics by "pinning" at grain boundaries with a secondary phase, pores, inclusions etc, [2]. Other studies

have focused on the thermodynamics of the phenomenon, attempting to lower this grain boundary energy by including alloying elements that segregate to intercrystalline regions[2–4]. The grain boundary energy, γ, may calculated[3,4] using Equation 7.

$$\gamma = \gamma_0 - \Gamma(\Delta H^{seg} + kT \ln X) \qquad \text{Equation 7}$$

γ_0 is the grain boundary energy of the pure base metal, Γ is the specific solute excess at the grain boundaries, ΔH^{seg} is the enthalpy of segregation, and kTlnX is the entropic contribution of segregation with solute composition X. ΔH^{seg} for binary alloys can be estimated using Miedema-type thermodynamic models. Murdoch and Schuh have compared the results of their Miedema-type model and the results of other models and experiments[3]. The results are consistent in showing that ΔH^{seg} may be positive for many binary alloy systems. The combined effects of a highly positive ΔH^{seg} and raising the entropy[4] through segregation lead to decreasing grain boundary energy γ with increasing grain boundary solute excess Γ. The result is lower γ and a reduced thermodynamic driving force for the growth of grains.

Renk, et. al. used atom probe tomography (APT) to investigate whether nanocrystalline 316L stainless steel processed by HPT shows evidence of grain boundary segregation. The results suggest that Si and, to a lesser extent, Cr, Mo, and C, segregate to grain boundaries and form secondary particles after annealing at 550 °C [17]. Figure 8 shows the increase in Γ_{Si} (the excess of Si solute at the grain boundaries) after annealing. Figure 9 shows the hardness increased with increasing temperatures up to about 550 °C, above which hardness dropped considerably. It was

suggested that grain growth was suppressed from room temperature to 550 °C but also grain growth was partly responsible for the precipitous drop in hardness above that temperature[17].

Therefore, segregation of solutes in nanocrystalline 316L and the stabilizing of grain boundaries may be possible in some temperature ranges. Further study is needed to find the temperatures at which the material retains its nanocrystalline structure. Further study also needs to determine the properties of the nanocrystalline material, such as oxidation rates and hardness.

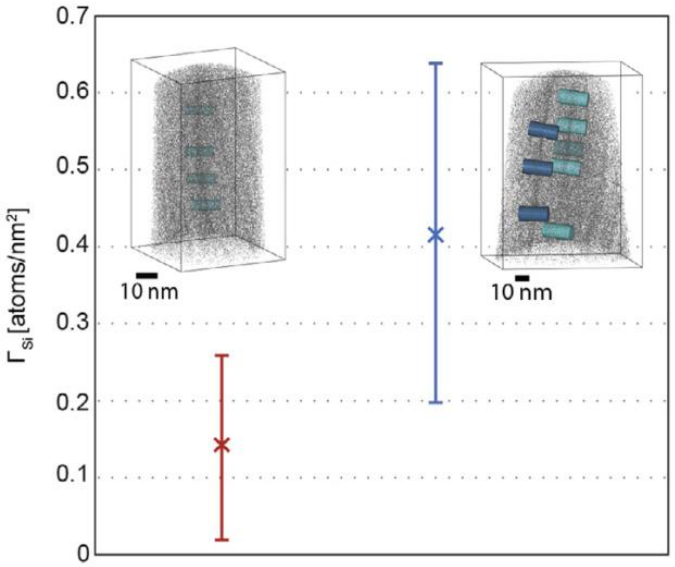

Figure 8 – Γ_{Si} before (red) and after (blue) annealing at 550°C for 1.5 hrs[17]

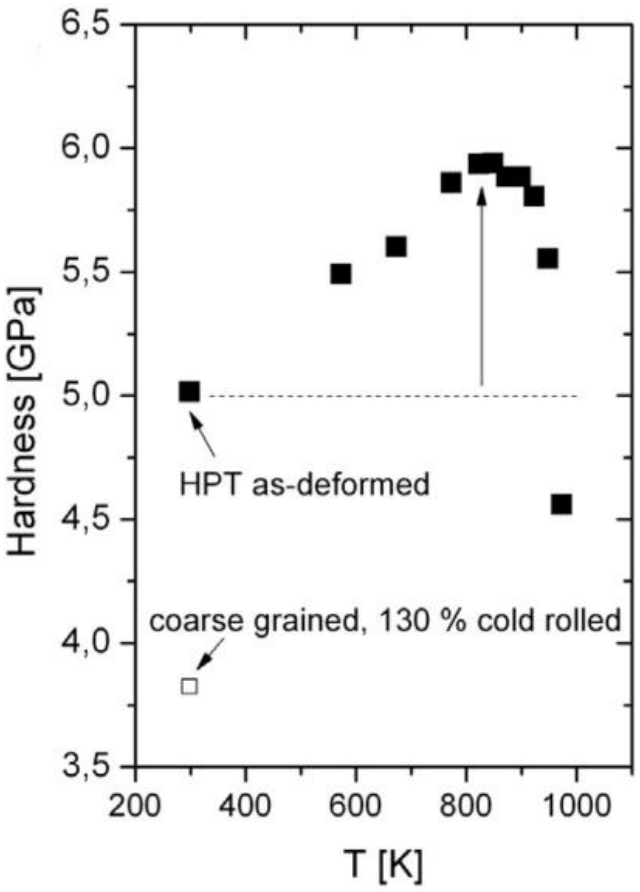

Figure 9 – Hardness vs. annealing temperature (30 min. annealing time)

3.4 Areas for Further Study

Based on the literature review following are the possibilities for future studies/experiments:

- Oxidation rates of nanocrystalline and polycrystalline 316L stainless steel formed by HPT should be measured at a range of temperatures to compare their performance.
- SEM/EDS should be used to characterize oxide scale thicknesses and compositions. Results should relate to the measured oxidation rates.
- Grain growth should be measured at several temperatures.

- Hardness measurements of HPT samples can be performed before and after exposure to elevated temperatures. Hardness may roughly correspond to grain size.
- Effects of HPT on oxidation resistance should be compared with effects of other processing methods.
- Microscopy of oxide scales can be used to find grain size of the oxide.
- The composition of the scales may be characterized using techniques such as XPS to determine if Cr content is affected by the grain size.
- Grain boundaries can be examined to find evidence of solute segregation.

In summary, the literature suggests that grain refinement by high pressure torsion may be an effective way to increase the oxidation resistance of 316L, but more experimental evidence is required to determine this conclusively.

3.5 Concluding remarks

It may be possible that high pressure torsion could be used to produce nanocrystalline 316L stainless steel materials with reduced oxidation kinetics. The nanocrystalline materials possess a relatively large density of grain boundaries and triple points where solute may rapidly diffuse. The literature shows that enhanced diffusion of Cr in materials forming external chromia scales typically imparts improved resistance to high temperature oxidation. However, metal oxidation rates are affected by a number of factors and so experimental results are needed to determine if HPT can indeed produce 316L with lower oxidation rates. It is also not necessarily clear if the refined grain size will be stable, although previous studies have claimed that the nanocrystalline grains can be retained at elevated temperatures.

4.0 Experimental Method

As described in the preceding literature review, it is hypothesized that nanocrystalline (nc) 316L stainless steel formed by high pressure torsion may exhibit improved high temperature oxidation resistance in comparison to its microcrystalline (mc) counterpart. 316L forms an external chromia scale during oxidation and the higher density of grain boundaries and triple points in the nanocrystalline material may facilitate diffusion of Cr to the surface to form a more protective oxide layer[1,8]. However, there is relatively little data on high temperature oxidation of such materials formed by HPT. Additionally, there is a lack of experimental data on the stability of grain size of the material formed using this processing method. This study aims to answer these questions on the effects of HPT on high temperature behavior of 316L. The nanocrystalline 316L samples used in the following experiments were processed by HPT and characterized by Dr. A. Hohenwarter, University of Leoben, Austria[17]. Focus of present work was to study the oxidation behavior and methodology is presented in this section.

4.1 Oxidation Tests

Samples of both nc and mc 316L stainless steel were ground to 1200 grit on SiC paper and rinsed with acetone. Each sample was dimensioned with a micrometer so that surface area could be calculated. Each sample's weight was measured using a microbalance (weighed each sample 3 times to confirm accurate numbers) so that initial weights were known. Samples were placed in ceramic boats in an upright position so that both front and back faces were exposed to the environment. The furnace was set for the desired temperature (either 600, 800, or 900°C). These experiments were performed in a box furnace, shown in Figures 10 and 11. The ceramic boats

containing the metal samples were placed inside the furnace only after the target temperature was reached. When weight measurements were to be taken (1, 2, and 4 hours after beginning of test and then once every 24 hours), the furnace door was opened and the ceramic boats removed with tongs and placed on a tray filled with ceramic. To avoid equilibrium cooling, the furnace temperature was not ramped down prior to removal. After samples cooled down to room temperature, they were weighed on the same microbalance and using the same procedure used to obtain initial weights. After weights were recorded, the samples were returned to the furnace at the target temperature. This method of measuring oxidation rates can introduce thermal stresses, and thus cracking and spalling, due to cyclic cooling and heating[7]. However, this is nevertheless a generally accepted method because it does not significantly alter the oxidation process[7].

Mean weight change (Δm = weight at time t -initial weight) divided by surface area (A), $\Delta m/A$, was plotted against time for nc and mc samples at each temperature. The square of $\Delta m/A$ versus time was then plotted. The slope of the trend line provided the parabolic oxidation rate constant and the coefficient of determination, R^2, indicated how well a parabolic trend line fit the data. Standard deviations of the weight measurements were calculated to estimate the error of the measurements.

4.2 Characterization of the oxide scale

After oxidation tests were complete, two samples, one nc and one mc, had their cross sections examined using a Hitachi TM3000 Scanning Electron Microscopy (SEM) coupled with Electron Dispersive X-Ray Spectroscopy (EDXS). Samples were mounted in an epoxy resin with the surface to be inspected lying face-down. After hardening, they were ground with SiC paper up to

1200 grit and then polished with 1 micron alumina powder on a nylon cloth. Epoxy was also ground away on the opposite side to expose bare metal, helping provide electrical conductivity with the SEM sample holder. Micrographs were taken using secondary electron mode and EDXS was performed on areas approximately 10μm x 10μm. Features that were examined include the oxide scales, bulk metal, and any secondary phases when present.

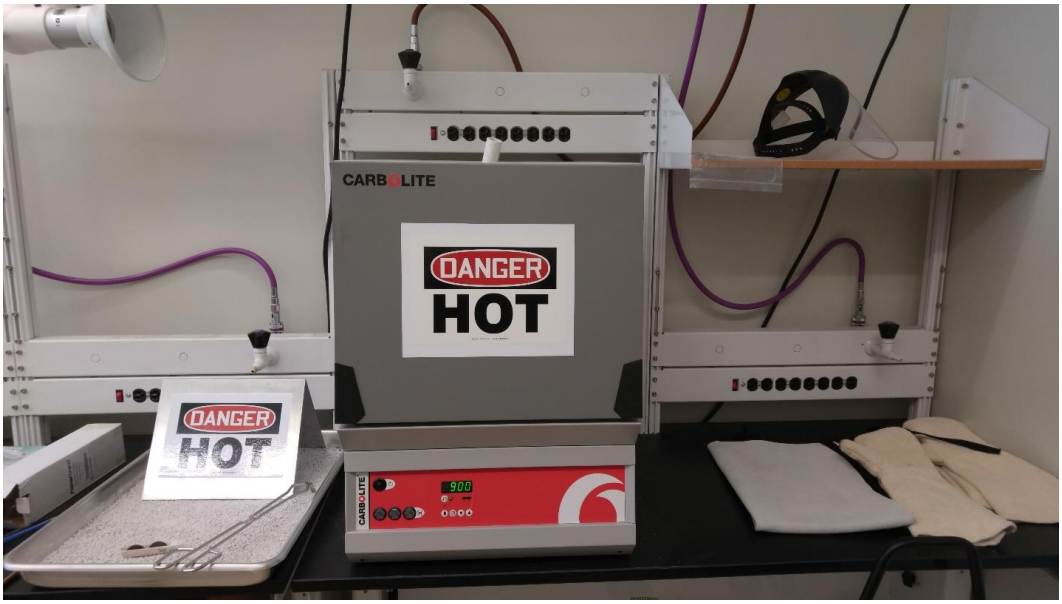

Figure 10 – Experimental setup including hot tray (left), furnace, and PPE (right) including face mask, leather apron, and insulating gloves

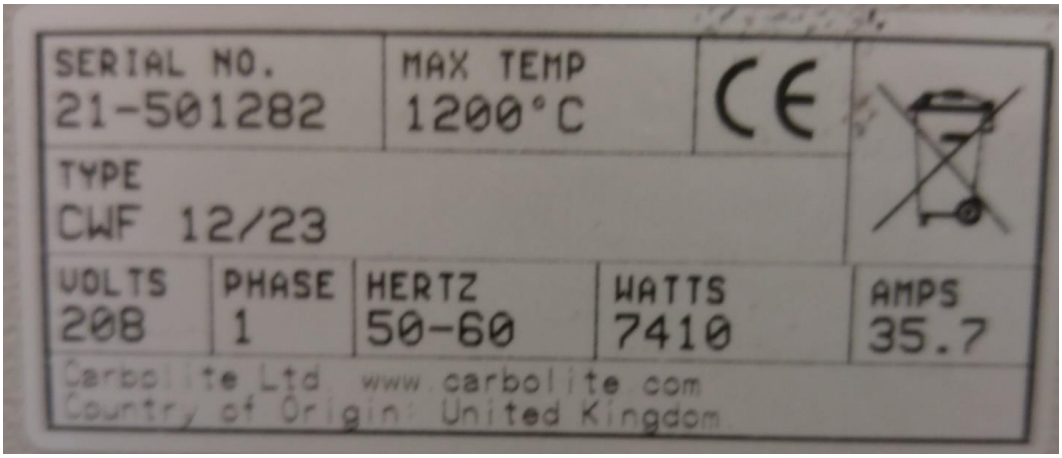

Figure 11 – Furnace specifications

5.0 Data and Results

5.1 Oxidation tests at 800 °C

Figure 12 and Figure 13 show the change in weight of nanocrystalline and microcrystalline samples at a temperature of 800 °C. At this temperature, the mc samples appeared to oxidize at a faster rate than the nc samples. However, the difference in weight change between nc and mc is barely above one standard deviation (indicated by the error bars in Figure 12), so it is uncertain whether this difference is significant or not. The data in Figure 13 show a roughly linear relationship between square of weight change and time, suggesting parabolic oxidation kinetics. The slopes of the trend lines provide an estimate of oxidation rates in $mg^2\,cm^{-4}\,hr^{-1}$.

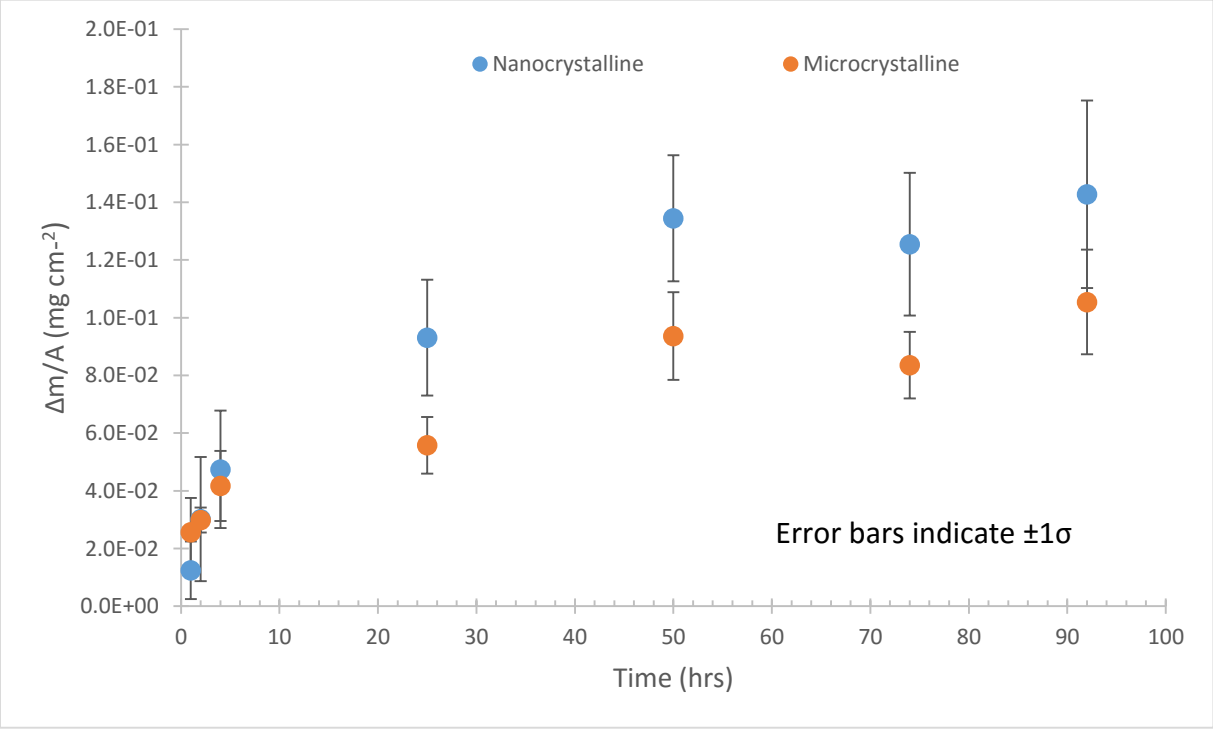

Figure 12 - Weight change per area ($\Delta m/A$) at 800°C

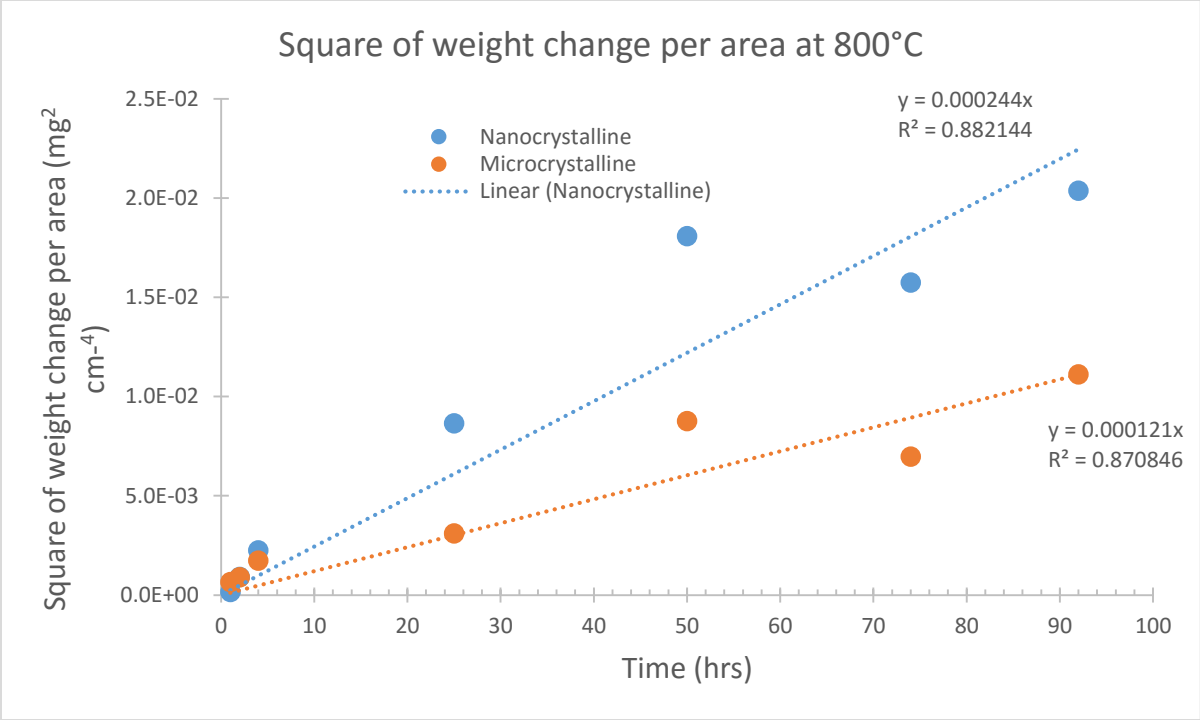

Figure 13 - Square of weight change per area at 800°C

Figure 14 shows SEM images of the nc cross-section (left) and mc cross-section (right) for the samples oxidized at 800°C for 96 h. A scale layer is visible in the nc alloy but not in the mc alloy. Mass gain data indicates presence of an oxide layer in both nc and mc alloys. The scale developed on mc alloys may have been accidentally removed during sample preparation and further experiments are required to reach any conclusion. Figure 15 shows EDXS maps suggesting that the scale developed on nc alloy is Cr-rich, likely Cr_2O_3, which is expected (as explained previously).

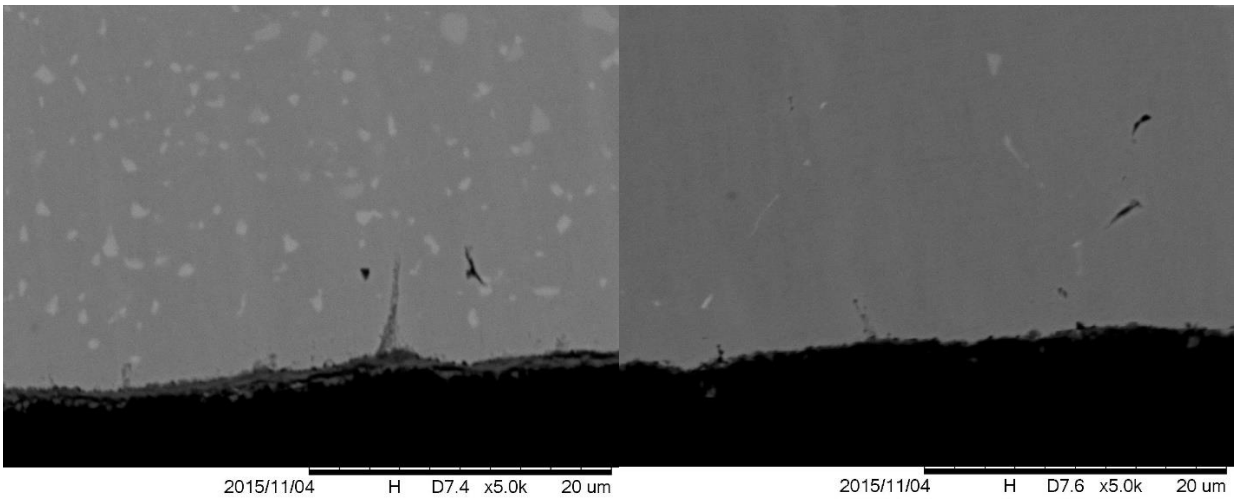

Figure 14 - SEM images of nc (left) and mc (right) samples oxidized at 800°C, 5000x

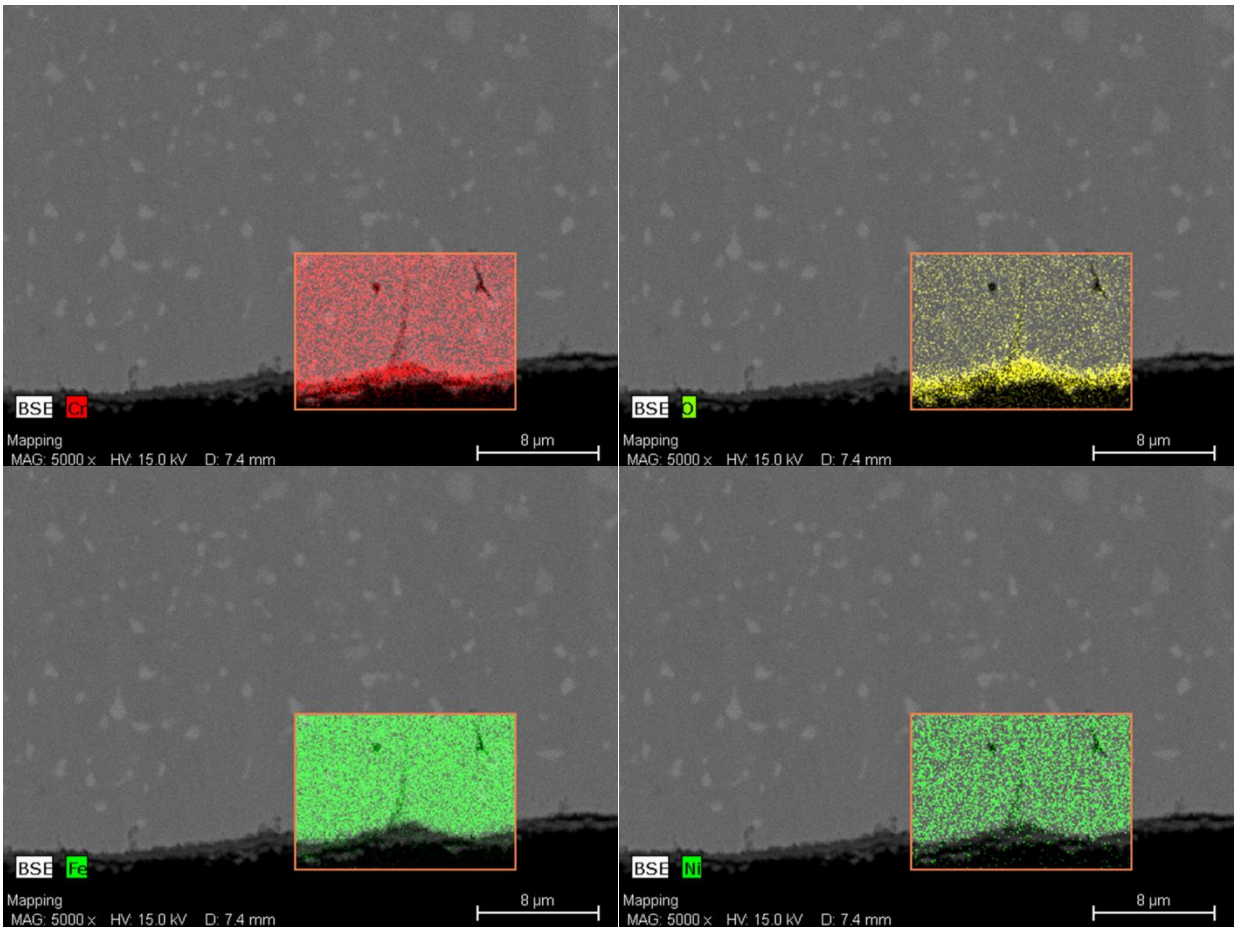

Figure 15 - EDXS maps for (clockwise, from top left) Cr, O, Ni, and Fe in the nc sample, 5000x

In both the nc and mc samples at 800°C, secondary phases (appearing bright) are visible throughout the bulk of the materials. Figure 16 shows that these phases are enriched in Mo and S. Phases of the essentially the same composition are visible in the nc sample (see Figure 14). These phases were not present in cross-sections of samples exposed to 900°C or 600°C. The Mo and S peaks overlap at around 2.3 keV. The only other peak that overlaps near this energy is Pb^{24}, which is very unlikely to be present. The exact composition and reason for these phases remains unknown.

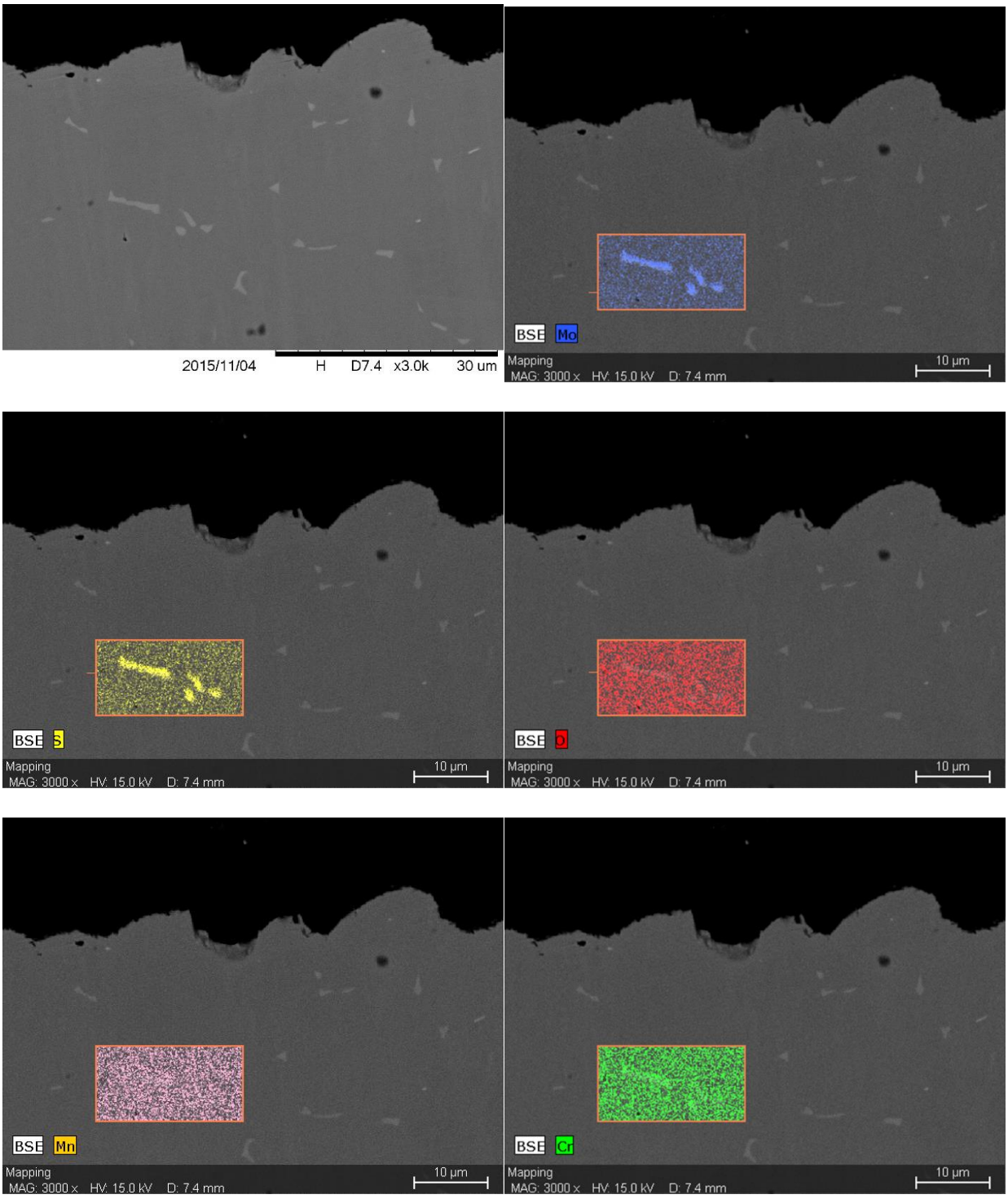

Figure 16 - EDXS maps of the light secondary phases in the mc 800°C sample (composition of phases in nc sample are nearly identical), 3000x

One interesting observation is that the nc 316L has a higher density of these phases than the mc 316L does. Also, the phases in the nc sample are more circular while the phases in the mc sample are more elongated. The reason of the formation of these phases at 800°C is not yet understood, but will be considered in future experiments (see section "Future Work"). The effect of grain size and diffusivity on the density and morphology of these phases remains a topic to be investigated.

5.2 Oxidation tests at 900 °C

Figure 17 shows the weight change per area for samples oxidized at 900°C. Due to time constraints, only one nc sample and one mc sample were tested and so standard deviations of the measurements could not be calculated. However, the oxidation tests at 900°C will be repeated with multiple samples in the near future (see section "Future Work"). Figure 18 shows the square of weight change per area and, as with tests at 800°C, suggests parabolic oxidation kinetics.

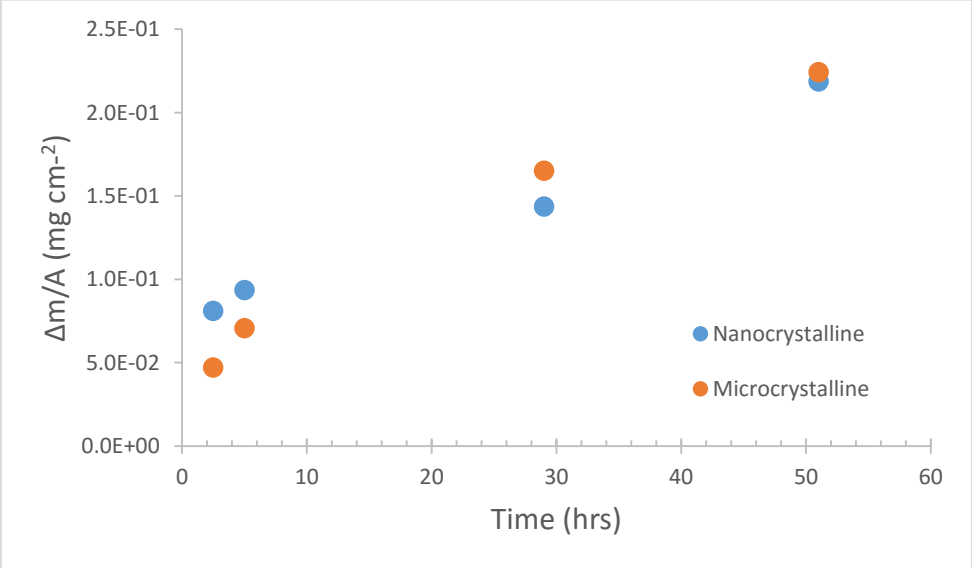

Figure 17 - Weight change per area at 900°C, test 1

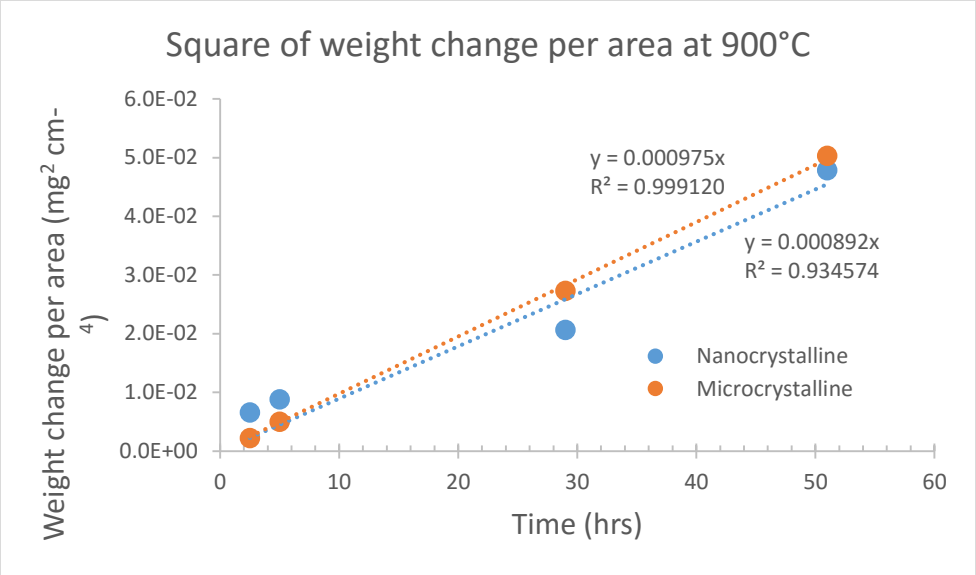

Figure 18 - Square of weight change per area at 900°C

Oxidation at 900 °C was repeated. This time the nc sample exhibited parabolic kinetics, but the mc sample did not. In fact, the mc sample had negative weight change for the first 75 hours, suggesting it was experiencing spallation. The nc parabolic rate of 7.31×10^{-4} $mg^2\,cm^{-4}$ is in reasonable agreement with the prior test.

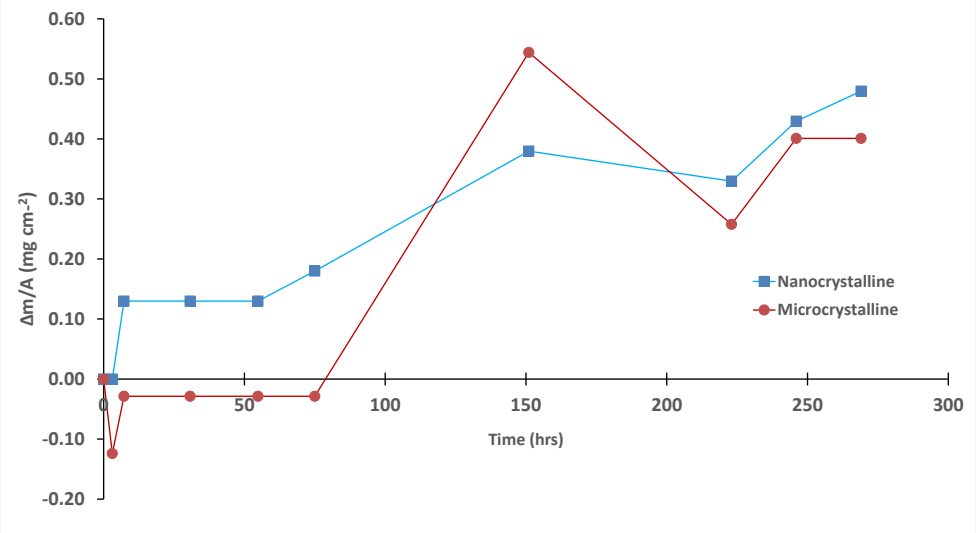

Figure 19 – Δm/A for test 2 at 900 °C (test 2)

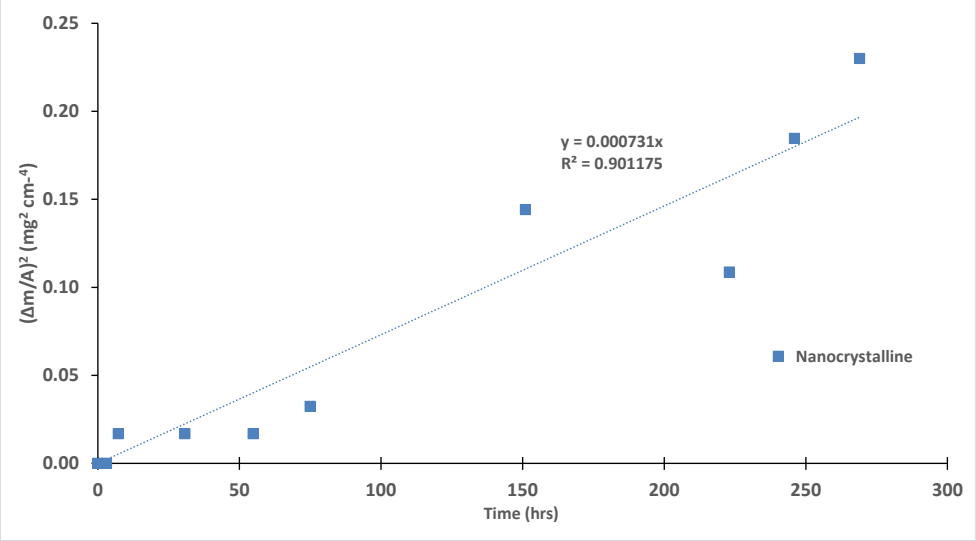

Figure 20 – $(\Delta m/A)^2$ for nc alloy from test 2 at 900 °C (test 2)

The cross-sections of the alloys oxidized at 900 °C showed no phases like those in the alloys oxidized at 800 °C. The scales could not be characterized as the SEM images showed the oxides were torn off the substrate during sample preparation. However, top-down images of the surface oxides were obtained. In Figure 21, no obvious difference in the morphology of the scales can be seen. The SEM used did not have sufficient resolution to provide a clear image beyond 5000x, so future studies with higher quality equipment may reveal useful data in the future. Both nc and mc samples had similar chromia compositions, as shown in Figure 22 and Figure 23.

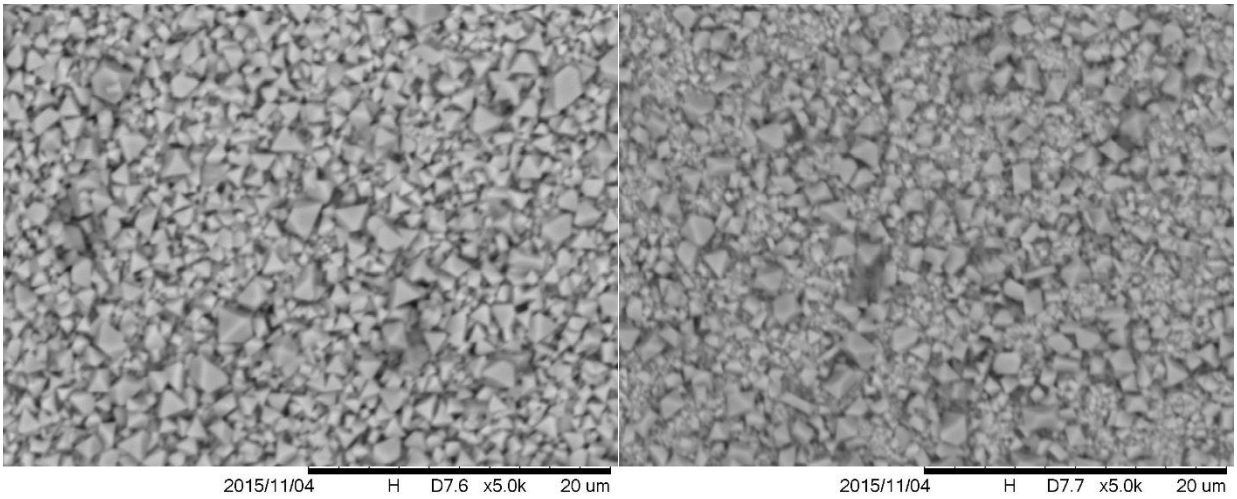

Figure 21 - Top-down SEM images of mc (left) and nc (right) oxide scales grown at 900 °C

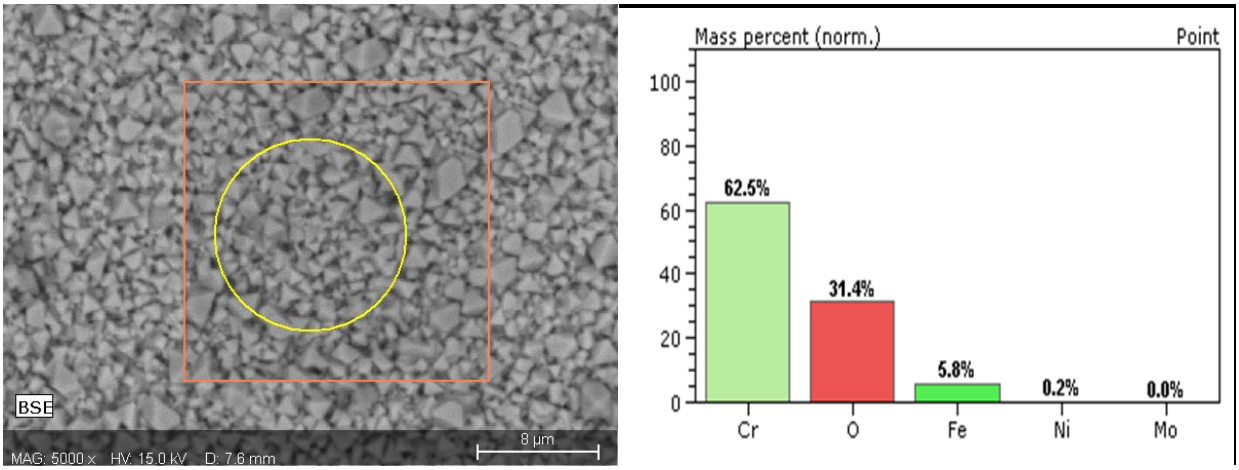

Figure 22 - EDXS analysis (right) of an area (left) on the mc 900 °C scale

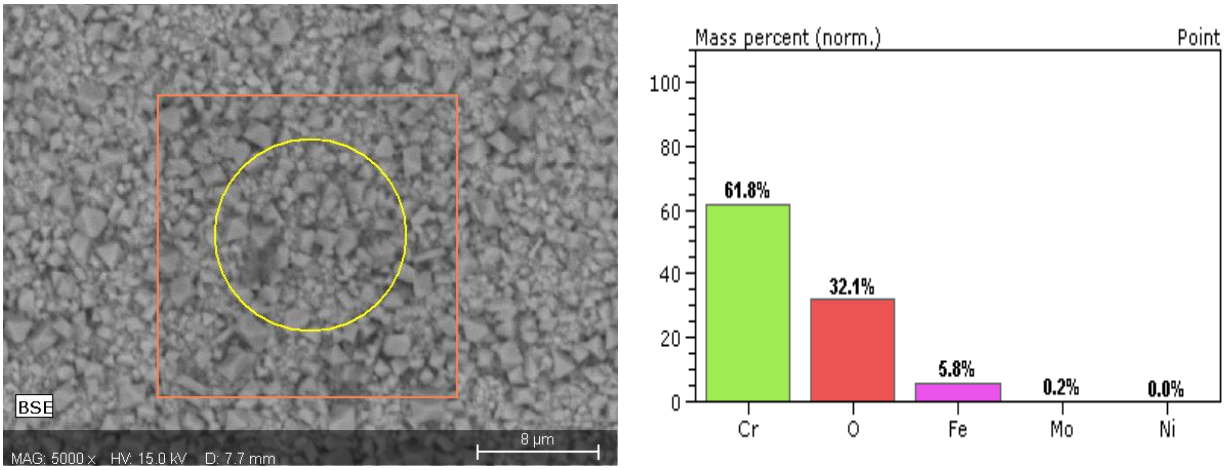

Figure 23 - EDXS analysis (right) of an area (left) on the nc 900 C scale, 5000x

Visual inspections (Figure 22) and optical microscopy (Figure 23) of the the oxidized SS316L revealed spalling in both samples and that spalling appears to be more severe in the unprocessed, microcrystalline sample after 90 hours of oxidation.

Figure 24 – More spallation products were found near the microcrystalline sample (right) than near the nanocrystalline sample (left)

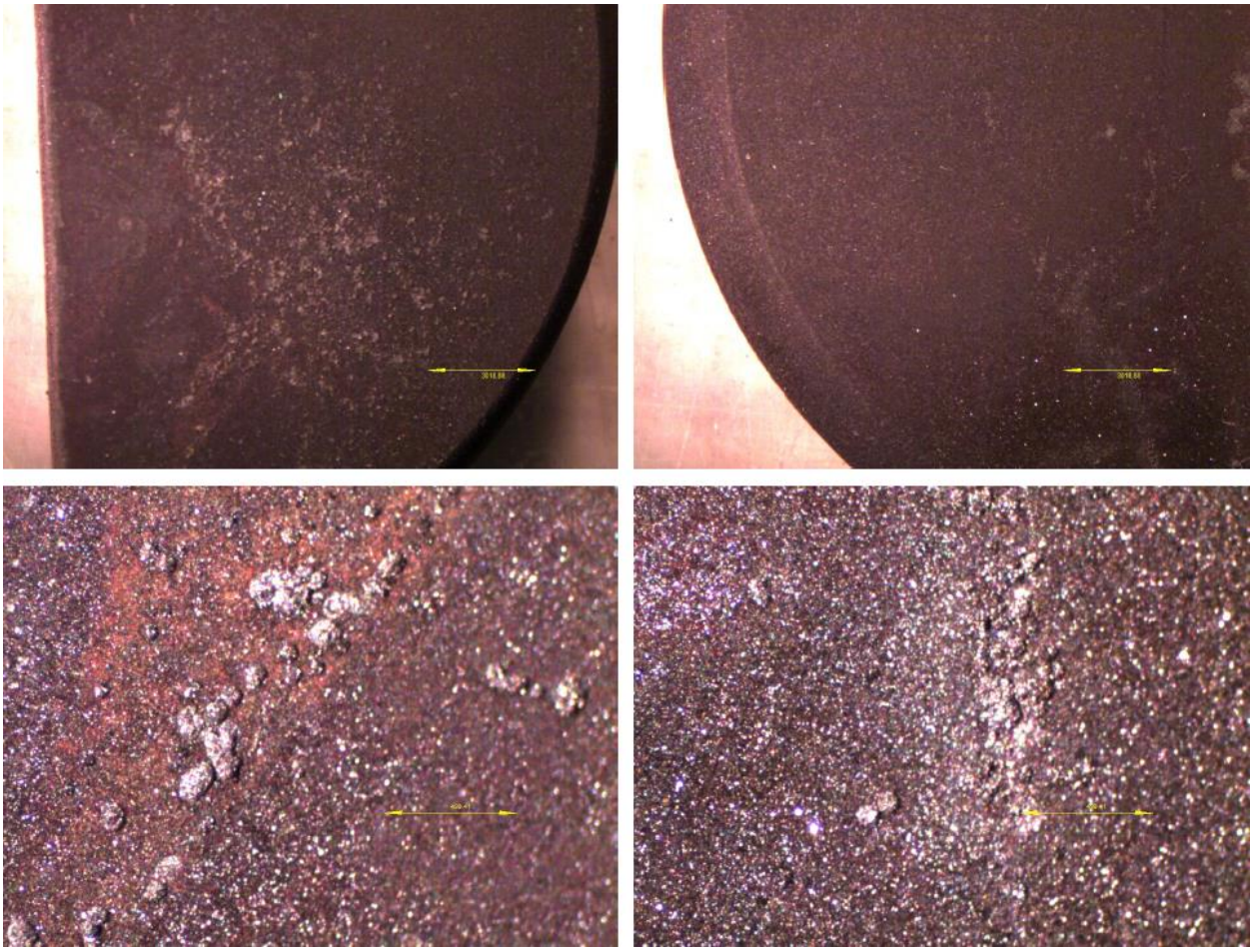

Figure 25- Optical microscope images at 6.7x (top) and 50x (bottom). Scale bar is in micrometers. Note how the grey, metal spallation regions are more widespread on the microcrystalline sample (left) than the nanocrystalline sample (right)

Heat treatments were performed on these materials. While these tests are not the focus of this project, they unexpectedly revealed relevant results. Heat treatment took place for 1 hour in the same furnace used for oxidation tests. Several temperatures were used, but the highest temperature (1000 °C) yielded the most interesting results. Images with the Lyra 3 TESCAN SEM show cracking in the oxide scale developed on microcrystalline sample but none in the nanocrystalline sample. These results are consistent with the other findings of greater spallation/cracking of the scale on the microcrystalline substrate.

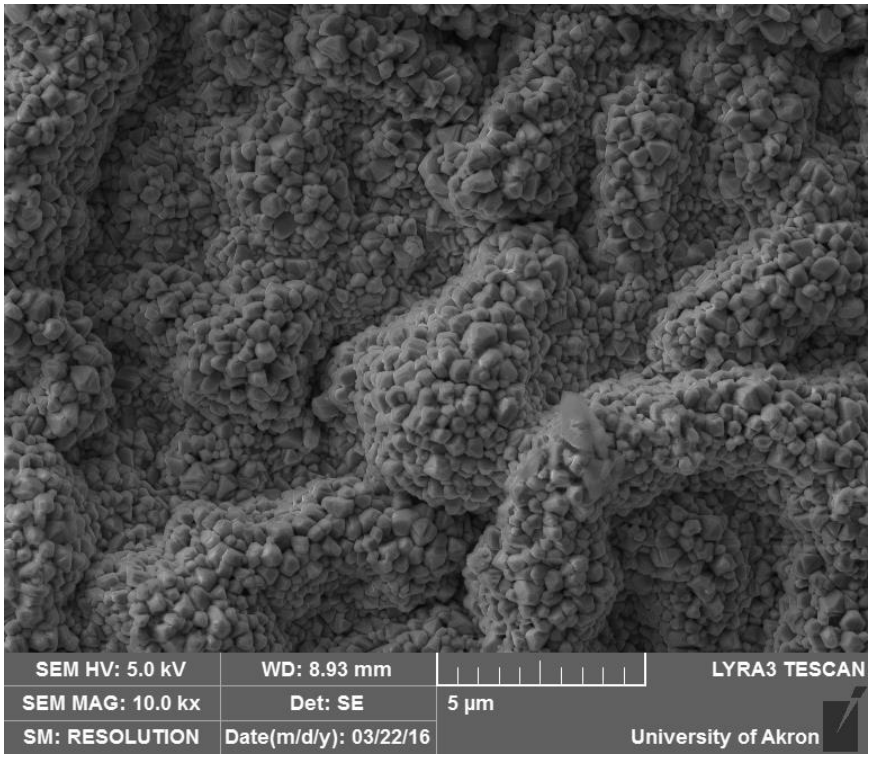

Figure 26 – No cracks were found on the nc sample after heat treating 1 hr at 1000 °C

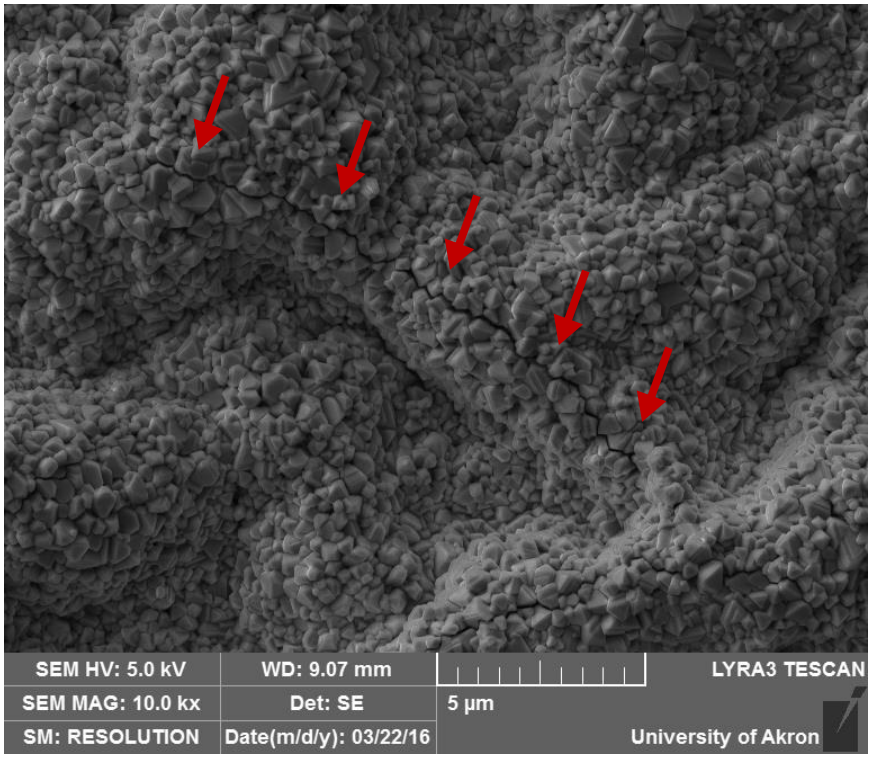

Figure 27 – Crack on the mc sample after heat treating 1 hr at 1000 °C. Cracks are marked by arrows.

5.3 Oxidation tests at 600 °C

Oxidation tests were also performed at 600 °C, but the weight changes were fractions of a milligram and likely within instrumental error. The data are not accurate representations of oxidation kinetics but are shown in Figure 28 for completeness. In the future, a higher total mass of steel samples may be used so that the measured weight change is larger than instrumental error.

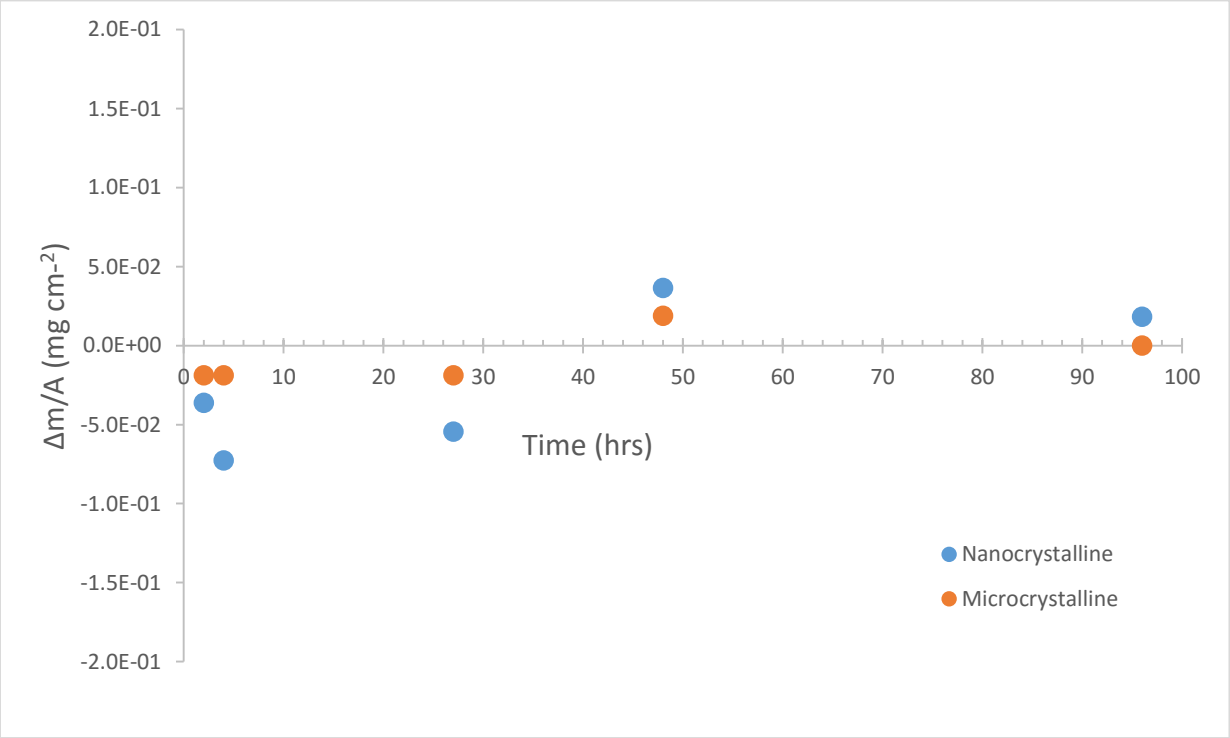

Figure 28 - Weight change per unit area at 600°

6.0 Discussion

A summary of all weight change data at obtained at 800 and 900 °C is presented in Table 1. The values in Table *1* were obtained from the trend lines in Figure 30. k_p is the parabolic oxidation rate and the R^2 value indicates how well the data fit the trend line and thus how closely the data follows a parabolic rate law. Based on the data, the hypothesis that using HPT to process type 316L stainless steel will result in improved oxidation resistance has not been verified. Nanocrystalline steel has performed about equally or even worse than mc steel in the experiments performed.

Table 1 - Summary of oxidation kinetics at 800 °C and 900 °C

Material	Temperature (°C)	k_p ($mg^2cm^{-4}hr^{-1}$)	R^2
Nanocrystalline SS316L	800	2.44×10^{-04}	0.8821
Microcrystalline SS316L	800	1.21×10^{-04}	0.8708
Nanocrystalline SS316L	900	8.92×10^{-04}	0.9346
Microcrystalline SS316L	900	9.75×10^{-04}	0.9346

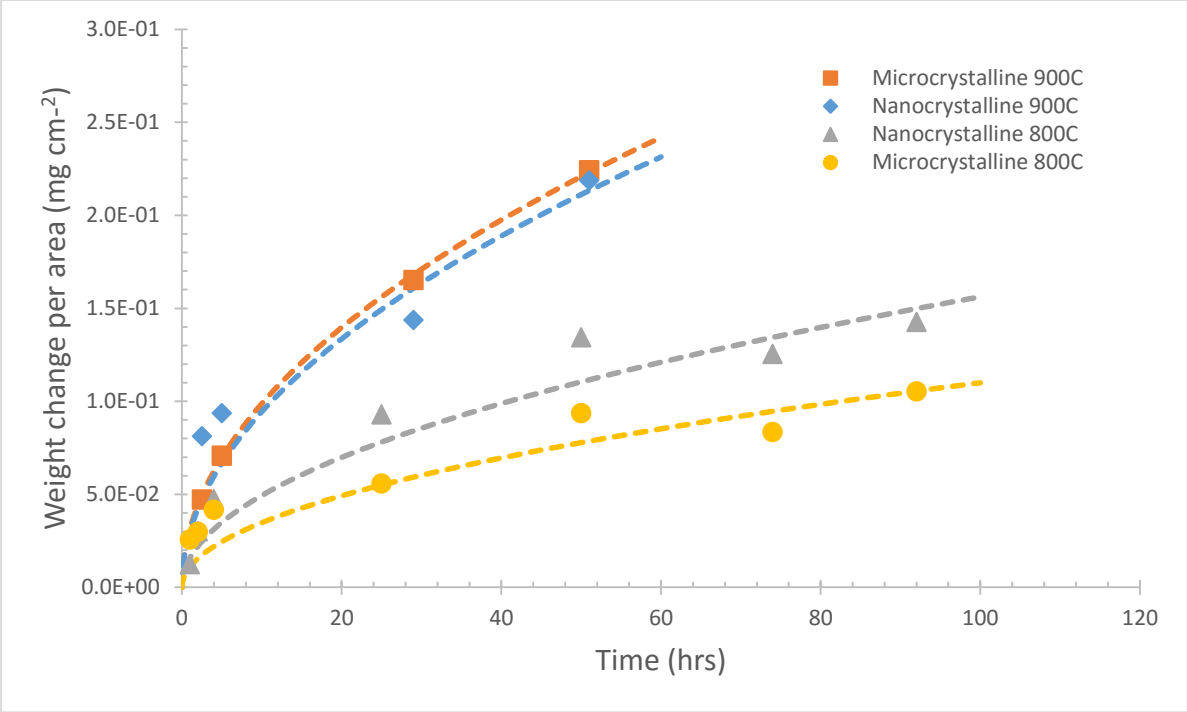

Figure 29 - Weight change per area at 800°C and 900°C

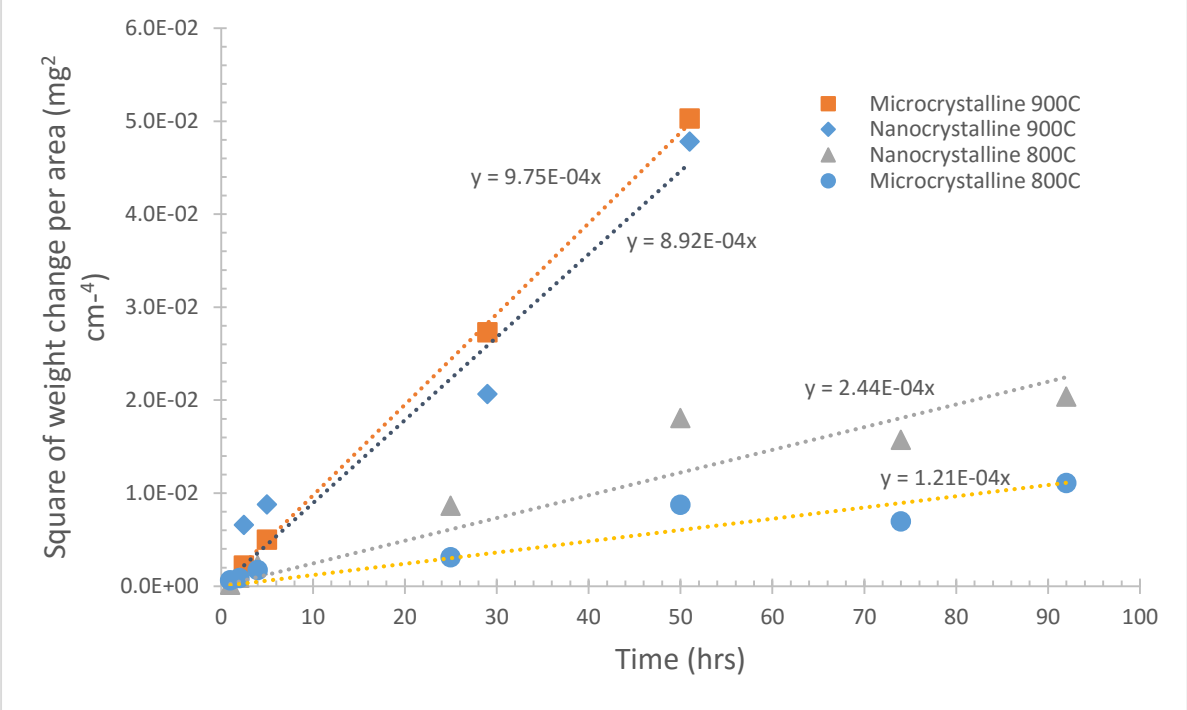

Figure 30 - Square of weight change per area at 800C and 900C

More work needs to be done, but so far there is no evidence of significant improvement in the oxidation resistance of the nanocrystalline 316L except an indication of the improved spallation resistance. In fact, at 800 °C the nanocrystalline 316L showed faster weight gain than the microcrystalline 316L samples (though the difference may not necessarily be significant). However, it is possible the weight measurements are not accurate due to spalling of oxide scales. While no significant spallation was observed, even tiny amounts of spallation could significantly affect results because changes in mass were in the range of milligrams to tenths of a milligram. Experiments in the future should make use of continuous Thermogravimetric Analysis (TGA). Continuous TGA measurements would allow the recording of spallation events as sudden decreases in weight[7]. TGA was not used because the equipment was not yet available, but future work may make use of this technique.

So far, the data do not show significant differences in scale morphology and composition between nc and mc materials. SEM and EDXS show that an external chromia scale forms on both materials, as expected. Unexpectedly, both materials form secondary phases at 800 °C that EDXS identifies as molybdenum sulfide. The composition appears the same in both materials, though there is a higher density of phases in the nc material than the mc material. Also, the phases in the nc material are rounder than those in the mc material, which are more elongated. This difference might be attributed to differences in grain size and thus diffusivity of solutes, but more data is required to study this relationship. The reason for the formation of secondary phases at this temperature is not yet known and will remain a topic of investigation in the future.

If future experiments (preferably using TGA, better sample preparation and FIB to prevent loss of the scales from the cross-sections, and higher resolution SEM equipment) confirm that there is no significant difference in oxidation rates, there could be several possible explanations. One could be that grain growth in the nc material is significant and the nanocrystalline structure is lost. Another is that the some properties of the nanocrystalline material cause faster oxidation kinetics, such as a finer scale enhancing diffusion of oxygen to the substrate (as discussed previously in the literature review section). A third possibility is that HPT introduces some detrimental parameter (such as chemistry, environmental condition, etc.) that is unique to that processing method and is not present in other methods such as high-energy ball milling. This may explain the inconsistency between these results and those reported in the literature, which typically focus on other processing methods.

7.0 Conclusions

In summary, the following conclusions can be made:

- More work is needed, but preliminary results fail to show significant difference in oxidation rates between nc and mc 316L materials.
- At high temperatures, both materials appear to form external chromia scales similar in composition and morphology.
- Visual inspections suggest that scales on the nanocrystalline substrate are less prone to cracking and spallation than scales on the microcrystalline material.

- Both materials formed secondary phases at 800 °C. EDXS suggests they are molybdenum sulfide. In the nc material, there is a greater density of the phases and they are more round than those in the mc material.

8.0 Future Work

More experiments needed to be done than what could be completed in one semester. Weight change experiments should be repeated for reproducibility purposes, preferably using TGA to get continuous data and record spallation events. A greater surface area of samples could be used in each experiment so that the change in mass is more easily measured. Experiments should be performed at other temperatures, such as 950 °C and 1000 °C, to provide a more complete understanding of high temperature behavior. If the results show an Arrhenius relationship, the activation energy for oxidation could be calculated for each material[7]. Afterwards, cross sections will be examined using better SEM equipment and FIB may be used to produce higher quality cross-sections. It is essential to measure grain size before and after exposure to high temperatures. X-ray diffraction (XRD) could be used because Scherrer's Equation states there is an inverse relationship between peak width and grain size[25]. Microhardness testing can be used as a rough indication of grain size and will provide useful data on mechanical properties of the alloys. Finally, a technique such as XPS can be used to measure concentration gradients of solutes, particularly Cr, to give an understanding of diffusion processes occurring during oxidation.

The following has been proposed to take place spring semester 2016:

- Oxidation experiments will be repeated for reproducibility and, if time permits, at 950 °C and 1000 °C.
- Microhardness measurements will be used as rough indicators of grain size and to provide data on changes in mechanical properties.

XPS will be used to measure concentration gradients of Cr near the surface. Sputtering with Ar will allow analysis of the composition at multiple distances from the surface.

9.0 Acknowledgements

I would like to thank Javier Esquivel, for attending the lab while doing oxidation experiments and also taking SEM images. I would also like to thank Tony (Dr. Anoton Hohenwarter) for providing the HPT samples.

10.0 Literature Cited

1. Raman, R. K. S., Gupta, R. K. & Koch, C. C. Resistance of nanocrystalline vis-à-vis microcrystalline Fe–Cr alloys to environmental degradation and challenges to their synthesis. *Philos. Mag.* **90,** 3233–3260 (2010).
2. Akbarpour, M. R. & Kim, H. S. Materials & Design Microstructure , grain growth , and hardness during annealing of nanocrystalline Cu powders synthesized via high energy mechanical milling. *Mater. Des.* **83,** 644–650 (2015).
3. Murdoch, H. A. & Schuh, C. A. Estimation of grain boundary segregation enthalpy and its role in stable nanocrystalline alloy design. *J. Mater. Res.* **28,** 2154–2163 (2013).
4. Greiner, J. *et al.* Design of Stable Nanocrystalline Alloys. *Science (80-.).* **337,** 951–954 (2012).
5. Jeong, G., Park, J., Kang, S. & Choi, H. Strategies to suppress grain growth of nanocrystalline aluminum. *Trans. Nonferrous Met. Soc. China* **24,** s112–s118 (2014).
6. Opila, E. High Temperature Materials Corrosion Challenges for Energy Conversion Technologies. *ECS Interface* **22,** 69–73 (2013).
7. Birks, N., Meier, G. H. & Pettit, F. S. *Introduction to the High-Temperature Oxidation of Metals*. (Cambridge University Press, 2006).
8. Gupta, R. K., Birbilis, N. & Zhang, J. in *Corrosion Resistance* (ed. Shih, H.) 213–238 (InTech, 2012).
9. Xia, Z. X., Zhang, C., Huang, X. F., Liu, W. B. & Yang, Z. G. Improve oxidation resistance at high temperature by nanocrystalline surface layer. *Sci. Rep.* **5,** 13027 (2015).
10. Journal, T., Caplan, D., Graham, M. J. & Cohen, M. Effect of Cold Work on the Oxidation of Nickel at High Temperature. **119,** (1969).
11. Chen, S., Jin, X. & Rong, L. Improvement in High Temperature Oxidation Resistance of 9 %Cr Ferritic–Martensitic Steel by Enhanced Diffusion of Mn. *Oxid. Met.* (2015). doi:10.1007/s11085-015-9596-6
12. Gupta, R. K. & Birbilis, N. The influence of nanocrystalline structure and processing route on

corrosion of stainless steel: A review. *Corros. Sci.* **92,** (2015).

13. Zhilyaev, A. & Langdon, T. Using high-pressure torsion for metal processing: Fundamentals and applications. *Prog. Mater. Sci.* **53,** 893–979 (2008).

14. Scheriau, S., Zhang, Z., Kleber, S. & Pippan, R. Deformation mechanisms of a modified 316L austenitic steel subjected to high pressure torsion. *Mater. Sci. Eng. A* **528,** 2776–2786 (2011).

15. Zhilyaev, A. . *et al.* Experimental parameters influencing grain refinement and microstructural evolution during high-pressure torsion. *Acta Mater.* **51,** 753–765 (2003).

16. Liddicoat, P. V *et al.* Nanostructural hierarchy increases the strength of aluminium alloys. *Nat. Commun.* **1,** 63 (2010).

17. Renk, O. *et al.* Increasing the strength of nanocrystalline steels by annealing: Is segregation necessary? *Scr. Mater.* **95,** 27–30 (2015).

18. Han, Z. *et al.* Comparison of the oxidation behavior of nanocrystalline and coarse-grain copper. *Oxid. Met.* **63,** 261–275 (2005).

19. Wang, S. G., Sun, M., Han, H. B., Long, K. & Zhang, Z. D. The high-temperature oxidation of bulk nanocrystalline 304 stainless steel in air. *Corros. Sci.* **72,** 64–72 (2013).

20. Palumbo, G., Thorpe, S. J. & Aust, K. T. On the contribution of triple junctions to the structure and properties of nanocrystalline materials. *Scr. Metall. Mater.* **24,** 1347–1350 (1990).

21. Wu, L. & Yang, Z. Oxidation behaviour of Mg–2.1Gd–1.1Y–0.82Zn–0.11Zr alloy at high temperatures. *J. Alloys Compd.* **626,** 194–202 (2015).

22. Mahesh, B. V., Singh Raman, R. K., Scattergood, R. O. & Koch, C. C. Fe-Cr-Ni-Zr alloys with bi-modal grain size distribution: Synthesis, mechanical properties and oxidation resistance. *Mater. Sci. Eng. A* **574,** 235–242 (2013).

23. Kotan, H. Materials Science & Engineering A Microstructural evolution of 316L stainless steels with yttrium addition after mechanical milling and heat treatment. *Mater. Sci. Eng. A* **647,** 136–143 (2015).

24. Bruker Corporation. Periodic Table of Elements - A4. at <https://www.bruker.com/fileadmin/user_upload/8-PDF-Docs/X-rayDiffraction_ElementalAnalysis/HH-XRF/Misc/Periodic_Table_and_X-ray_Energies.pdf>

25. Uvarov, V. & Popov, I. Metrological characterization of X-ray diffraction methods at different acquisition geometries for determination of crystallite size in nano-scale materials. *Mater. Charact.* **85,** 111–123 (2013).

Appendix A: Raw Data for Tests at 800°C

Weights after 1 hr					
Sample	Weight 1	Weight 2	Weight 3	Weight avg.	Weight change per Area (mg cm^{-2})
nc3	5.0698	5.0700	5.0701	5.0700	0.0000E+00
nc4	5.8018	5.8018	5.8018	5.8018	1.2972E-02
nc5	6.1821	6.1822	6.1822	6.1822	2.4461E-02
mc3	6.0053	6.0054	6.0053	6.0053	1.2202E-02
mc4	8.3438	8.3438	8.3438	8.3438	4.0869E-02
mc5	7.1057	7.1058	7.1057	7.1057	2.4030E-02
Weights after 2 hr					
Sample	Weight 1	Weight 2	Weight 3	Weight avg.	Weight change per Area (mg cm^{-2})
nc3	5.0701	5.0700	5.0699	5.0700	4.1672E-02
nc4	5.8016	5.8019	5.8017	5.8017	0.0000E+00
nc5	6.1822	6.1822	6.1823	6.1822	4.8922E-02
mc3	6.0054	6.0053	6.0054	6.0054	2.4405E-02
mc4	8.3438	8.3437	8.3438	8.3438	3.5030E-02
mc5	7.1057	7.1058	7.1057	7.1057	3.0038E-02
Weights after 4 hr					
Sample	Weight 1	Weight 2	Weight 3	Weight avg.	Weight change per Area (mg cm^{-2})
nc3	5.0699	5.0701	5.0702	5.0701	5.5563E-02
nc4	5.8018	5.8019	5.8018	5.8018	1.9459E-02
nc5	6.1823	6.1824	6.1823	6.1823	6.7268E-02
mc3	6.0055	6.0055	6.0053	6.0054	3.6607E-02
mc4	8.3439	8.3439	8.3439	8.3439	5.8384E-02
mc5	7.1057	7.1057	7.1058	7.1057	3.0038E-02
Weights after 25 hr					
Sample	Weight 1	Weight 2	Weight 3	Weight avg.	Weight change per Area (mg cm^{-2})
nc3	5.0702	5.0703	5.0704	5.0703	1.0418E-01
nc4	5.8021	5.8020	5.8021	5.8021	6.4862E-02
nc5	6.1826	6.1826	6.1825	6.1826	1.1007E-01
mc3	6.0056	6.0054	6.0057	6.0056	6.1012E-02
mc4	8.3438	8.3439	8.3441	8.3439	6.4222E-02
mc5	7.1058	7.1057	7.1059	7.1058	4.2053E-02

Weights after 50 hr					
Sample	Weight 1	Weight 2	Weight 3	Weight avg.	Weight change per Area (mg cm^{-2})
nc3	5.0705	5.0705	5.0706	5.0705	1.5280E-01
nc4	5.8023	5.8022	5.8023	5.8023	1.0378E-01
nc5	6.1828	6.1827	6.1828	6.1828	1.4677E-01
mc3	6.0058	6.0058	6.0058	6.0058	1.0372E-01
mc4	8.3442	8.3441	8.3442	8.3442	1.0509E-01
mc5	7.1059	7.1060	7.1060	7.1060	7.2091E-02
Weights after 74 hr					
Sample	Weight 1	Weight 2	Weight 3	Weight avg.	Weight change per Area (mg cm^{-2})
nc3	5.0704	5.0705	5.0705	5.0705	1.3891E-01
nc4	5.8022	5.8022	5.8022	5.8022	9.0807E-02
nc5	6.1827	6.1828	6.1828	6.1828	1.4677E-01
mc3	6.0058	6.0056	6.0056	6.0057	7.9315E-02
mc4	8.3442	8.3442	8.3440	8.3441	9.9252E-02
mc5	7.1059	7.1059	7.1061	7.1060	7.2091E-02
Weights after 92 hr					
Sample	Weight 1	Weight 2	Weight 3	Weight avg.	Weight change per Area (mg cm^{-2})
nc3	5.0705	5.0706	5.0706	5.0706	1.5974E-01
nc4	5.8021	5.8023	5.8023	5.8022	9.7294E-02
nc5	6.1829	6.1829	6.1829	6.1829	1.7123E-01
mc3	6.0058	6.0058	6.0058	6.0058	1.0372E-01
mc4	8.3443	8.3443	8.3443	8.3443	1.2844E-01
mc5	7.1060	7.1061	7.1060	7.1060	8.4106E-02

Appendix B: Raw Data for Tests at 900°C

Weights after 2.5 hr					
Sample	Weight 1	Weight 2	Weight 3	Weight avg.	Weight change per Area (mg cm^{-2})
nc6	5.8862	5.8862	5.8862	5.8862	8.1231E-02
mc6	7.3455	7.3455	7.3456	7.3455	4.7210E-02
Weights after 5 hr					
Sample	Weight 1	Weight 2	Weight 3	Weight avg.	Weight change per Area (mg cm^{-2})
nc6	5.8862	5.8863	5.8863	5.8863	9.3728E-02
mc6	7.3456	7.3457	7.3457	7.3457	7.0814E-02
Weights after 29 hr					
Sample	Weight 1	Weight 2	Weight 3	Weight avg.	Weight change per Area (mg cm^{-2})
nc6	5.8864	5.8866	5.8866	5.8865	1.4372E-01
mc6	7.3462	7.3462	7.3462	7.3462	1.6523E-01
Weights after 51 hr					
Sample	Weight 1	Weight 2	Weight 3	Weight avg.	Weight change per Area (mg cm^{-2})
nc6	5.8868	5.8870	5.8870	5.8869	2.1870E-01
mc6	7.3465	7.3466	7.3465	7.3465	2.2425E-01

Appendix C: Raw Data for Tests at 600°C

Weight (mg) Over Time								
	Elapsed Time (hrs)							
Sample	0	1	2	4	27	48	96	213
nc1	5.6139	5.6141						
nc2	5.9714		5.9712	5.9710	5.9711	5.9716	5.9715	5.9713
mc1	7.5939	7.5931						
mc2	7.0273		7.0272	7.0272	7.0272	7.0274	7.0273	7.0725